A Comparative Theoretical and Experimental Investigation on the Adsorption of Small Molecules on Anatase and Brookite Surfaces

by

Selisa F. Rollins

A Thesis Presented in Partial Fulfillment
of the Requirements for the Degree
Master of Science

Approved July 2012 by the
Graduate Supervisory Committee:

Jean M. Andino, Chair
Lenore L. Dai
Erica S. Forzani

ARIZONA STATE UNIVERSITY

December 2012

ABSTRACT

The mitigation and conversion of carbon dioxide (CO_2) to more useful carbon chemicals is a research topic that is at the forefront of current engineering and sustainability applications. Direct photocatalytic reduction of CO_2 with water (H_2O) vapor to C_1-C_4 hydrocarbons has significant potential in setting substantial groundwork for meeting the increasing energy demands with minimal environmental impact. Previous studies indicate that titanium dioxide (TiO_2) containing materials serve as the best photocatalyst for CO_2 and H_2O conversion to higher-value products. An understanding of the CO_2-H_2O reaction mechanism over TiO_2 materials allows one to increase the yield of certain products such as carbon monoxide (CO) and methane (CH_4). The basis of the work discussed in this thesis, investigates the interaction of small molecules (CO, CH_4,H_2O) over the least studied TiO_2 polymorph – brookite. Using the Gaussian03 computational chemistry software package, density functional theory (DFT) calculations were performed to investigate the adsorption behavior of CO, H_2O, and CH_4 gases on perfect and oxygen-deficient brookite TiO_2 (210) and anatase TiO_2 (101) surfaces. The most geometrically and energetically favorable configurations of these molecules on the TiO_2 surfaces were computed using the B3LYP/6-31+G(2df,p) functional/basis set. Calculations from this theoretical study indicate all three molecules adsorb more favorably onto the brookite TiO_2 (210) surface. Diffuse reflectance Fourier transform infrared spectroscopy (DRIFTS) was used to investigate the adsorption and desorption behavior of H_2O and CH_4 on Evonik P25 TiO_2. Results from the experimental studies and

theoretical work will serve as a significant basis for reaction prediction on brookite TiO_2 surfaces.

ACKNOWLEDGEMENTS

I wish to extend my deepest appreciation to my committee chair, Dr. Jean M. Andino, for her excellent guidance and ongoing support. I also wish to extend a gracious thank you to my committee members, Dr. Lenore L. Dai and Dr. Erica S. Forzani, for generously contributing their valuable time and expertise. I wish to thank past and present members of the Andino research laboratory: Dr. Eulalia Siu, Tingting Gao, Monique Rodriguez, Alejandro Castaneda, Meghan Moloney, Zach Berkson, and Phillip Logan for their support. I wish to acknowledge the Western Alliance to Expand Student Opportunities Bridge to the Doctorate (WAESOBD) program (NSF, cooperative agreement #HRD-1025879) for financial support throughout my graduate career. Lastly, I wish to thank my family for their unwavering support and love. To Mom, Dad, Isaiah, Ursula, Autumn, and Grandma, I extend a heartfelt thank you!

TABLE OF CONTENTS

LIST OF TABLES

LIST OF FIGURES

Figure Page

Figure Page

Figure Page

CHAPTER 1: INTRODUCTION

1.1 CO_2 Mitigation and Conversion to Higher-Value Products

According to the International Energy Outlook 2011 (IEO2011) published by the U.S. Energy Information Administration (EIA), global energy consumption is expected to increase by 53 percent from 2008 to 2035.[1] As illustrated in Figure 1.1-1, an exponential growth in energy demand is projected, where the global energy consumption in 2008 and 2035 are 505 quadrillion British thermal units (Btu) and 770 quadrillion Btu respectively.

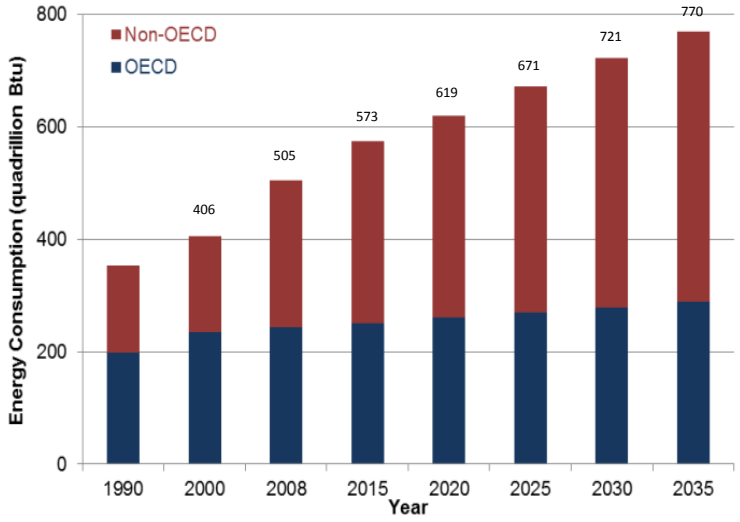

Figure 1.1-1 Historical and projected global energy consumption in Organization for Economic Cooperation and Development (OECD) and non-OECD countries.[1]

The power generation industry utilizes three types of sources - fossil fuels, nuclear energy, and renewable energy.[1] At present, approximately 83 percent of global energy originates from fossil fuels. Fossil fuels are non-renewable and encompass a range of commodities: coal, crude oil, and natural gas. Upon

combustion, fossil fuels emit excessive amounts of particulate matter and various polluting gases into the atmosphere, namely carbon dioxide (CO_2). By definition, CO_2 is classified as a greenhouse gas (GHG) pollutant that has a detrimental effect on the environment and global climate. In light of this matter, the strong correlation between anthropogenic activity (e.g. fossil fuel utilization), CO_2 emissions, and global warming has been well established within the scientific community.[2-5] Based off of EIA projections, global energy-related CO_2 emissions are expected to increase significantly (Figure 1.1-2) along with the increasing rate of demand for fossil resources (Figure 1.1-3).[1]

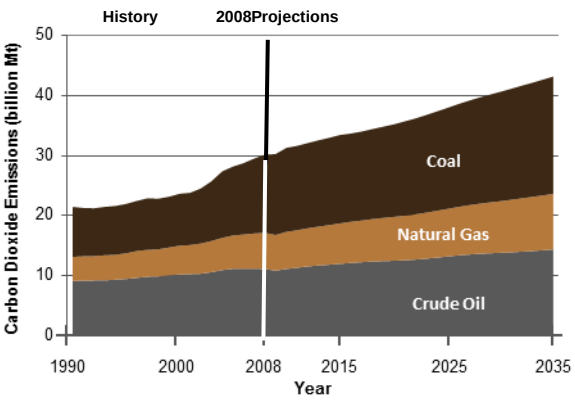

Figure 1.1-2 Historical and projected global energy-related emissions.[1]

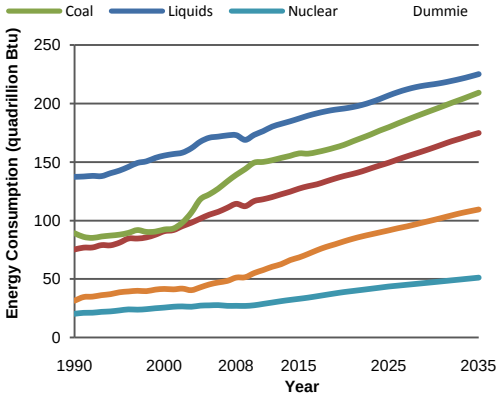

Figure 1.1-3 Projected global energy consumption by fuel type.[1]

The forecast for how long coal, crude oil, and natural gas resources will meet the projected energy demands is a widely disputed topic. Nonetheless, there is a consensus that the depletion of these resources is imminent (within decades).[6-8] The stronghold of fossil fuels in current global energy provision, as well as the detrimental effect they have on the environment (CO_2 emissions) is a significant

issue in need of immediate focus and resolution. Carbon capture and storage, CO_2 utilization in chemical processes, and CO_2 conversion to higher-value products are ways in which CO_2 emissions can be mitigated.[9, 10] Among the aforementioned approaches, CO_2 conversion to higher-value products (such as C_1-C_2 hydrocarbons) serves as a practical means for not only mitigating GHG emissions, but also addressing the forthcoming fossil fuel depletion crisis.[11] The most commonly implemented methods used for CO_2 conversion to higher-value products are shown in Table 1.1-4.[12-15]

Table 1.1-4 Summary of CO_2 Conversion to fuel methods

Technology	Reaction Medium	Products	Advantages	Challenges
Dry Reforming of Methane	CO_2/CH_4	carbon monoxide C_2 hydrocarbons, hydrogen	suitable conversion efficiency	highly endothermic reaction, requires high energy input, catalyst coking (deactivation)
Electrochemical Reduction	CO_2 saturated aqueous solution	carbon monoxide, formic acid, methane	energy efficient, direct or indirect conversion, inexpensive	mass transport limitations, short-term stability of catalyst and electrode material
Hydrogenation	CO_2/H_2	carbon monoxide, ethanol, formic acid, methane, methanol	suitable conversion efficiency	catalyst coking (deactivation)
Photocatalytic Reduction	CO_2/H_2O vapor	carbon monoxide, formic acid, formaldehyde, hydrogen, methane	abundance of energy source (sunlight), direct conversion, inexpensive	low product yields

Among these methods, photocatalytic reduction of CO_2 in the presence of water vapor (H_2O) is currently the most appealing due to its relatively inexpensive cost and novel experimental setup.[15, 16] For example, sunlight – a continuous and readily available source – is the only energy input needed to carry out many photocatalytic reactions.[17] Despite the various challenges associated with this method (e.g. low product yields, poor understanding of reaction mechanisms, etc.), direct photocatalytic conversion of CO_2 and H_2O vapor to higher order hydrocarbons is one of the most promising technologies to set substantial groundwork for meeting the increasing energy demands with minimal environmental impact.[18, 19]

1.2 Metal Oxides in Photocatalysis

Photocatalytic activity can be exhibited by a wide variety of materials – primarily semiconducting metal oxides.[17] The surface of a metal oxide consists of an ordered assortment of *Lewis* acid-base centers in which metal cations (M^{n+}) are bounded to oxygen anions (O^{2-}). Metal oxides with semiconducting properties contain free electrons which help to facilitate chemisorption and reduction-oxidation (redox) reactions of organic molecules.[20] Photocatalytic reactions over a semiconducting metal oxide are initiated by the absorbance of ultraviolet (UV) or visible photon energies equal to or greater than the metal oxide's band gap. Upon photon absorption, a valence band (VB) electron is promoted to the conduction band (CB) – thereafter, moving freely throughout the metal oxide's lattice. The promotion of an electron to the CB generally leads to reduction

reactions; in which the generated electron can react with electron-acceptor groups or molecules present on the metal oxide's surface. Likewise, the electron-hole or unoccupied electron state in the VB can react with electron-donor groups or molecules present on the metal oxide's surface – resulting in oxidation reactions.[21]

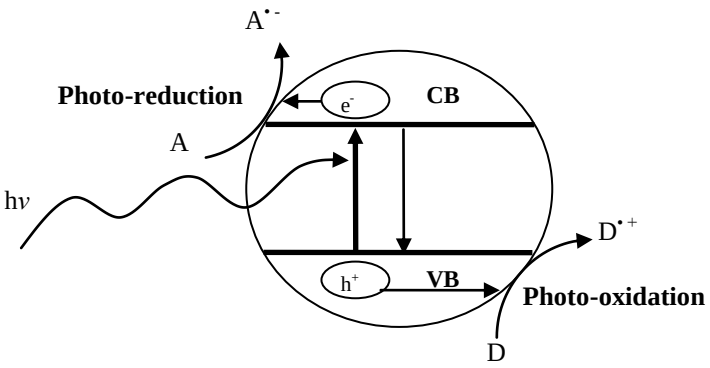

Figure 1.2-1 Schematic of photocatalytic activation of a semiconductor. CB: conduction band; VB:valence band; A:electron-accepting species; D:electron-donating species.[22, 23]

CHAPTER 2: PHOTOCATALYTIC CONVERSION OF CO_2 TO FUELS

2.1 Conversion of CO_2 and H_2O to C_1-C_2 Hydrocarbons

A 1972 published study by Fujishima *et al.* investigated the photo-splitting of H_2O at a semiconductor electrode.[24] Among the various oxide semiconductors that were utilized in this study, the titanium dioxide (TiO_2) electrode demonstrated the best ability to induce electrochemical photolysis of H_2O. The basis of this research demonstrated that H_2O could be decomposed by visible light into oxygen and hydrogen products. By way of this research, the following reaction schemes were established:

(1) $$TiO_2 + 2\,h\nu \rightarrow 2\,e^- + 2\,h^+$$

(2) $$2\,h^+ + H_2O \rightarrow \tfrac{1}{2}\,O_2 + 2\,H^+$$

(3) $$2\,e^- + 2\,H^+ \rightarrow H_2$$

Overall Reaction:

(4) $$H_2O + 2\,h\nu \rightarrow \tfrac{1}{2}\,O_2 + H_2$$

Since the discovery of the photolysis of H_2O on TiO_2, photocatalysis research has expanded significantly. For instance, the production of fuels by way of photocatalysis has been a predominant area of interest.[25] In 1979, Inoue and collaborators were the first researchers to experimentally demonstrate photoelectrocatalytic reduction of CO_2 to organic compounds using

photosensitive semiconductor powders.[26] Gallium phosphide (GaP), titanium dioxide (TiO_2), tungsten trioxide (WO_3), and zinc oxide (ZnO) were among the various photocatalysts used to carry out the CO_2 reduction reaction and produce products such as formaldehyde (HCHO), formic acid (HCOOH), methanol (CH_3OH), and methane (CH_4).[27] In addition to the Inoue *et al.* study, extensive research with regard to CO_2 photocatalytic reduction to other valuable products has been conducted (as shown in Table 2.1-1). The predominant research studies have demonstrated that TiO_2 containing materials serve as the most suitable photocatalysts for carrying out this reaction.

Table 2.1-1 Review of CO_2 (with H_2O vapor) photocatalytic reduction reactions

Light Source	Photocatalyst	Products	Reference
UV	TiO_2 loaded zeolite	methanol	Anpo *et al.*[27]
UV	Ti containing SiO_2 film	methane and methanol	Ikeue *et al.*[28]
UV laser (λ=266 nm)	Ti-silicalite molecular sieve	carbon monoxide formaldehyde	*Ulagappam et al.*[29]
UV	TiO_2 powder	methane, hydrogen, carbon monoxide	Tan *et al.*[30]
UV	TiO_2 (P25 Degussa), ZrO_2	methane, ethane, carbon monoxide	Lo *et al.* [31]
UV (λ=365 nm)	MW-CNT supported TiO_2	ethanol, formic acid	Xia *et al.*[32]
UV (λ=365 nm)	Ag/Cu-TiO_2 coated optical fiber	methanol	Wu *et al.*[33]
natural sunlight	Cu, Pt co-catalyzed N-doped TiO_2 nanotubes	methane, other alkanes, olefins, Br-paraffins, H_2, carbon monoxide	Varghese *et al.*[34]

visible light (λ=420 nm)	CdSe/Pt/TiO_2 heterostructure	methane, methanol, carbon monoxide, hydrogen	Wang *et al.*[35]

2.2 Properties of TiO_2

There exist three polymorphic forms of TiO_2: anatase, brookite, and rutile. Anatase and rutile share the same tetragonal modification; wherein, chains of TiO_6 in an octahedral configuration share corners.[36, 37] On the contrary, brookite is orthorhombic in structure and has longer Ti—O bond lengths than anatase and rutile. In all three forms of TiO_2, each O atom is coordinated to three Ti atoms and Ti atoms are coordinated to six intermediate O atoms.[38]

Table 2.2-1. Crystal structure data of TiO_2 polymorphs[39]

	Anatase	**Brookite**	**Rutile**
Lattice Constants (Å)	a = b = 3.784 c = 9.515	a = 9.184 b = 5.447 c = 5.145	a = b = 4.5936 c = 2.9587
Ti—O bond length (Å)	1.937 1.965	1.87 ~ 2.04	1.949 1.980
O—Ti—O bond angle	77.7° 92.6°	77.0 ° ~ 105°	81.2° 90.0°

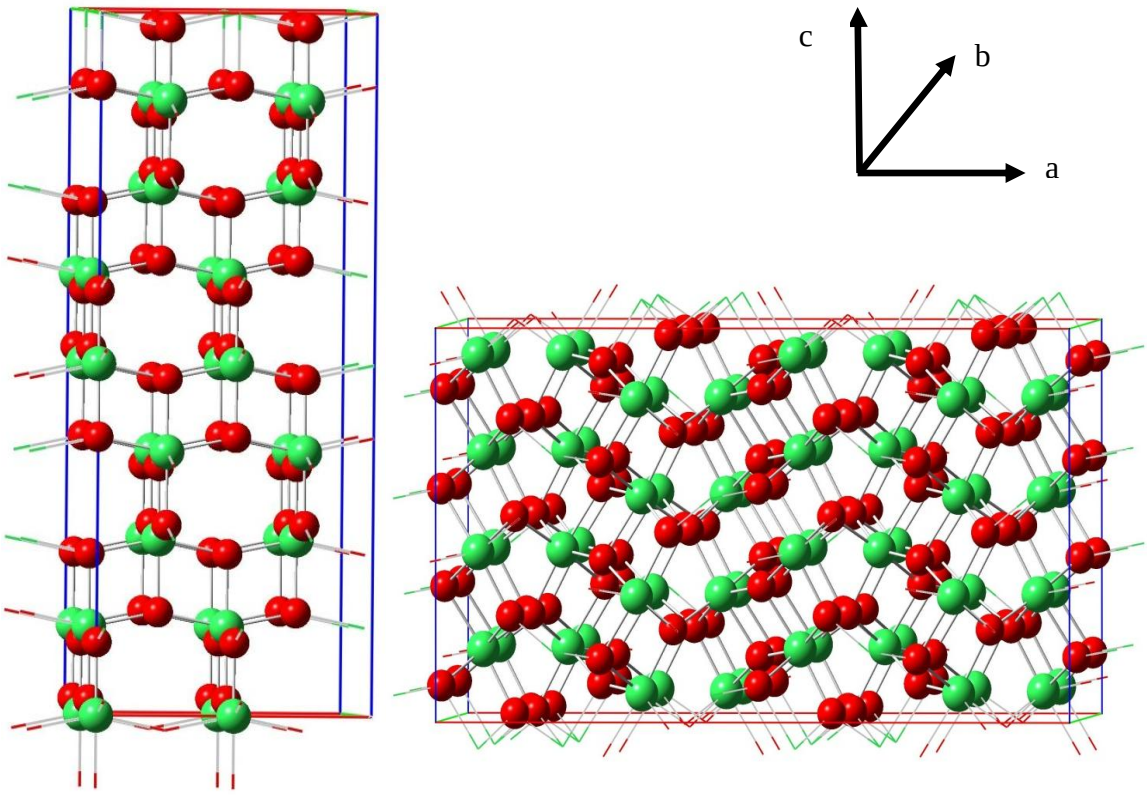

(a) (b)

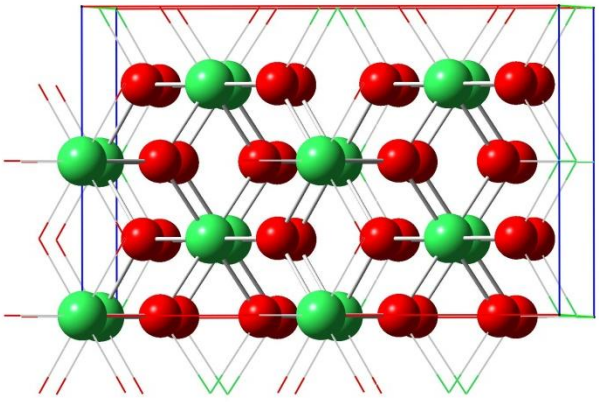

(c)

Figure 2.2-2 TiO_2 polymorphs: (a) anatase (tetragonal), (b) brookite (orthorhombic), (c) rutile (tetragonal); Ti atoms in green, O atoms in red.

Various literature suggest anatase, brookite, and rutile have estimated band gap energies of 3.24 eV, 3.27 eV, and 3.03 eV, respectively.[40] Among the three polymorphic structures of TiO_2, rutile is considered the most stable phase under ambient conditions; whereas anatase and brookite are metastable in nature.[36] According to literature, anatase is the most extensively studied polymorph of TiO_2 that exhibits high photocatalytic activity and selectivity and responds to a UV wavelength of approximately 382 nm.[41] Moreover, theoretical and experimental surface studies have shown the anatase TiO_2 (101) interface to be the most commonly exposed and thermodynamically stable surface for this polymorph.

Rutile has excitation wavelengths extending into the visible light range at 410 nm. However, rutile's photocatalytic activity is much less than that of anatase.[36, 41] Among the various rutile facets, the rutile TiO_2 (001) and (110) surfaces are the most photocatalytically active and thermodynamically stable, respectively.[42, 43] Brookite is the least studied phase of TiO_2, partly due to past difficulties in creating pure brookite samples.[44, 45] Brookite responds to a much shorter UV wavelength (372 nm) than that of anatase and rutile. In spite of its high activation energy input, brookite exhibits more photocatalytic activity than the anatase and rutile phases of TiO_2. The (210) surface is the most commonly exposed and stable facet of brookite TiO_2 that has a similar structural building as that of the anatase TiO_2 (101) surface.[46] Moreover, recent studies in the literature indicate the brookite TiO_2 (210) surface is more reactive than the anatase TiO_2 (101) surface.[46]

Practical applications of single-phase TiO_2 materials are significantly limited due to a variety of challenges. The main challenges include: low utilization of solar energy (due to wide band gaps) and rapid recombination of electron-hole pairs.[47] Various methods outlined in the literature have been implemented to address these challenges. For example, the development of mixed-phase TiO_2 nanoparticles has demonstrated significant potential in enhancing the photocatalytic activity of TiO_2.[30, 48-51] Evonik P25 TiO_2, a commercially available material consisting of approximately 75 percent anatase and 25 percent rutile, demonstrates enhanced photocatalytic activity.[48]

The explanation as to why mixed-phase TiO_2 materials exhibit enhanced photocatalytic activity is widely disputed. An electron paramagnetic resonance spectroscopy (EPR) study conducted by Hurum *et al.* expounds on the charge separation characteristics of Evonik P25 TiO_2; thus, helping to better explain why mixed phase materials demonstrate enhanced photocatalytic activity.[48] Observations from this experimental study were as follows:

- rutile extends the excitation wavelength of the photocatalyst into the visible light region of the electromagnetic spectrum
- electron transfer from rutile to anatase aids in reducing recombination rates
- structural arrangement of the rutile promotes "catalytic hotspots" at the anatase-rutile interface

In summary, this study established that interfacial trapping sites which do not exist in single phase TiO_2 is prevalent in mixed phased TiO_2 and helps to enhance

charge separation. A visual representation of this proposed model is shown in Figure 2.2-3.

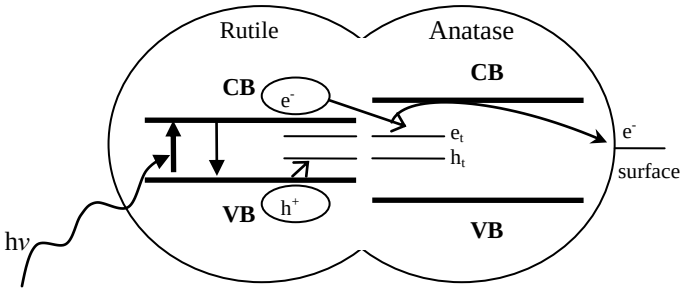

Figure 2.2-3 Proposed model of charge separation characteristics of mixed-phase composite material, Evonik P25 TiO_2.[48]

2.3 Experimental Investigations of Reaction Mechanisms on TiO_2

Studies from the literature suggest CO_2 reduction to higher-value products can be achieved via electrochemical, photochemical, photocatalytic, and photoelectrochemical methods. Reaction schemes for the electrochemical (aqueous-phase) reduction of CO_2 to hydrocarbons have been proposed in a variety of studies. For example, an experimental study conducted by Centi *et al.* concluded that the initial and most critical step in CO_2 reduction entails the formation of the CO_2^{-}.[25] This study proposed that CO_2^{-} formation eventually leads to one of the following:

- further reduction to chemisorbed carbon monoxide (CO)
- formation of the formate anion ($HCOO^-$)

Centi *el al.* assert that $HCOO^-$ can be further reduced (via interaction with four electrons and protons) to $:CH_2$ species adsorbed on the surface. The interaction of

:CH_2 with two electrons and protons can lead to methane (CH_4) formation. Conversely, the mechanism proposed by Centi *et al.* points out that two :CH_2 species can react with one another and form ethylene (C_2H_4). A more thorough review of this mechanism can be observed in Figure 2.3-1.

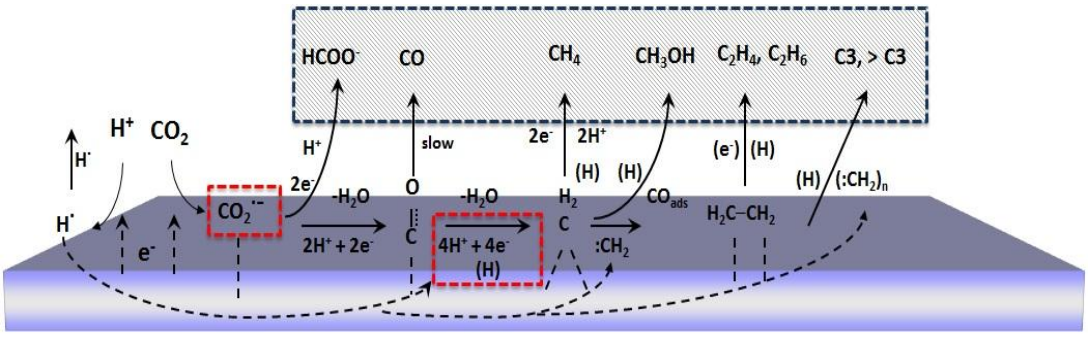

Figure 2.3-1 Simplified reaction mechanism of CO_2 reduction to hydrocarbons; reactants are boxed in red, products are boxed in blue.[25]

Carbon dioxide reduction via the photocatalytic method is novel approach wherein a solid-gas interaction ensues. Higher adsorption capacity and enhanced contact area are significant advantages the photocatalytic method has over the previously mentioned approaches. According to the literature, the photocatalytic reduction of CO_2 to hydrocarbons is considered a complex multistep reaction involving shared intermediates and multiple reaction pathways. It is imperative to note that by understanding the mechanism, one can mitigate the pathway of the reaction and drive the production of a particular product.

Extensive work in the realm of CO_2 photoreduction to high-value products has been conducted over the years. Anpo *et al.*'s 1995 study of the photocatalytic reduction of CO_2 (with H_2O vapor) on powdered TiO_2 catalysts provides insight as to how various reaction variables play a significant role in product formation.[52] Variables such as the type of catalyst being utilized, the reaction temperature, and the CO_2 to H_2O ratios were found to have a profound effect on the percent yield of certain products (i.e. CO, CH_3OH, and CH_4). For instance, it was determined that an increase in the ratio of H_2O to CO_2 enhanced the reactivity of the TiO_2 catalysts.[52]

An H_2O to CO_2 ratio of five was found to be the most optimal condition for yielding a higher yield of products.[52] Anything in excess of this ratio was shown to suppress rates of the photocatalytic reactions taking place in this study. In addition to product yield analyses, this work also included a proposed reaction mechanism for the photocatalytic reduction of CO_2 with H_2O on TiO_2. This reaction scheme is displayed in Figure 2.3-2.

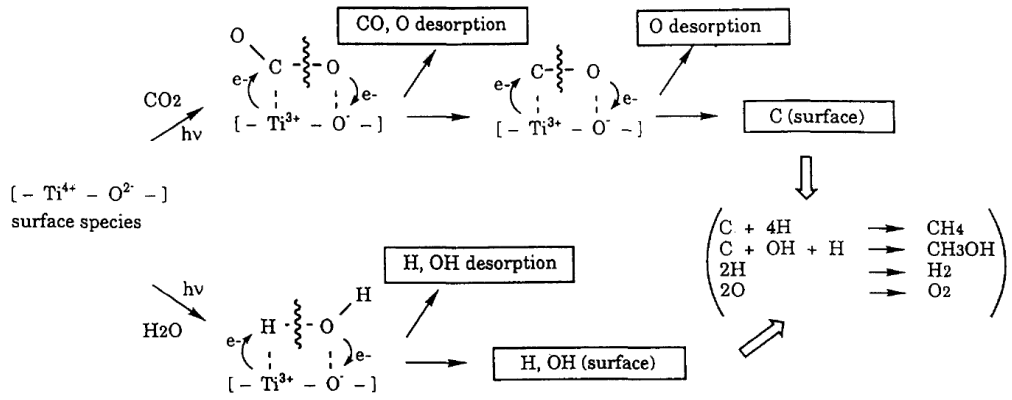

Figure 2.3-2 Anpo *et al.* schematic representation of the photocatalytic reduction of CO_2 with H_2O on anchored TiO_2.[52]

Just as in the previously discussed work by Centi *et al.*, various experimental studies have confirmed that the initial and most critical step in CO_2 photoreduction entails the formation of the CO_2^-.[53-55] The CO_2^- has a characteristically bent formation and is formed via interaction with an electron. Work conducted by Ramis *et al.* and Rasko *et al.* are the first reported experimental studies in which infrared (IR) spectral frequencies are uniquely assigned to various states of CO_2 (linear, bent, and carbonate) on TiO_2 nanoparticles.

2.4 Theoretical Investigations of Reaction Mechanisms on TiO_2 Catalysts

In addition to the aforementioned experimental work, various computational studies have been implemented to investigate CO_2 interaction and reduction on various TiO_2 surfaces.[47, 56-58] This in turn has led to a better

understanding of the reaction mechanisms as well as the development of more efficient TiO_2 catalysts. Work outlined in a series of publications by Indrakanti encompass quantum chemical modeling of ground and excited states of CO_2 on both stoichiometric and oxygen-deficient TiO_2 (anatase and rutile) surfaces.[47, 57, 59] Indrakanti's 2008 publication investigated the interaction properties (e.g. charge transfer and adsorption) of CO_2 on small clusters ($Ti_2O_9H_{10}$) extracted from the anatase TiO_2 (101), (010), and (001) surfaces.[57] Further, the theoretically calculated vibrational frequencies from this study were in agreement with experimentally observed IR frequencies of CO_2 reduction on anatase TiO_2.[53] Likewise, a computational study performed by He *et al.* sought to investigate different binding configurations of CO_2 on neutral, negatively charged, and oxygen-vacant anatase TiO_2 (101) cluster and periodic surfaces. Most importantly, this study demonstrated that CO_2^- formation occurs when adsorbed onto the negatively charged surface.

The indication of how a reactant (H_2O) and products (HCOOH, CO, CH_4, etc) of CO_2 photoreduction interact with the various TiO_2 polymorphs (anatase, brookite, rutile) contributes significantly to better understanding the reaction mechanism. A comparative DFT study on the adsorption behavior of H_2O and HCOOH on the anatase TiO_2 (101) and brookite TiO_2 (210) surfaces was previously conducted.[46] According to the literature, the anatase TiO_2 (101) and brookite TiO_2 (210) surfaces have the same structural build. As shown in Figure 2.4-1, 6-fold and neighboring 5-fold coordinated Ti atoms (Ti_{6c} and Ti_{5c}) atoms are exposed on the anatase TiO_2 (101). Likewise, 3-fold and 2-fold coordinated O

atoms (O_{3c} and O_{2c}) are also present on the surface. Considering how it's similar in structure to the anatase TiO_2 (101) surface, these reactive sites also apply to the brookite TiO_2 (210) surface.[44]

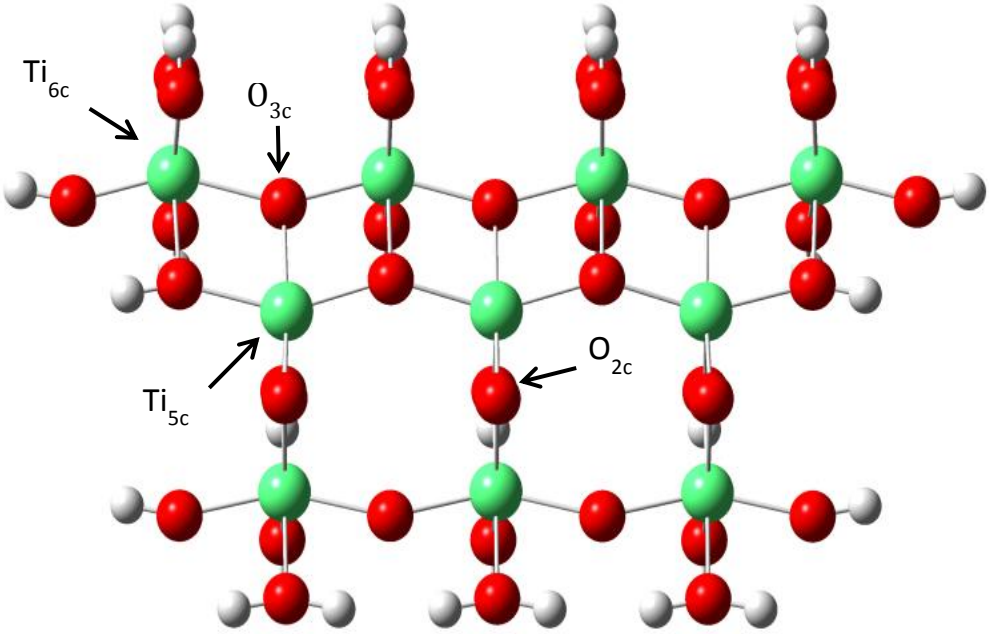

Figure 2.4-1 Atomic components of the structural units exposed on the anatase TiO_2 (101) surface.

Although the brookite TiO_2 (210) surface has the same structure as that of the anatase TiO_2 (101) surface, its form is orthorhombic and interatomic distances are slightly shorter.[46] Computational studies suggest that due to its structural features, the brookite TiO_2 (210) surface exhibits distinct activity for more favorable adsorption sites than the anatase TiO_2 (101) surface.[46, 60] In summary,

these various computational studies have helped to broaden the current understanding of the mechanisms of CO_2 photoreduction.

2.5 Research Objectives

Literature suggests that among the three forms of TiO_2, brookite is the least studied polymorph computationally and experimentally. The lack of experimental studies concerning brookite is in part due to it being the most difficult TiO_2 phase to synthesize.[60-62] Furthermore, brookite has been shown exhibit high photocatalytic activity – making it an ideal catalyst for executing photochemical reactions. As previously mentioned in Section 2.3, published work provided an account (from a theoretical standpoint) of the significant potential brookite may have in catalytic and photocatalytic applications.[46] Not until recently has there been a mounting interest in investigating the photocatalytic activity of brookite-containing mixed-phase TiO_2 nanoparticles.[46, 60, 63-65]

The scope of the research discussed in this thesis entails executing a comparative theoretical study of the adsorption behavior of small molecules (CO, H_2O, and CH_4) on the anatase TiO_2 (101) and brookite TiO_2 (210) surfaces. This work will provide significant insight towards the reaction mechanisms of CO_2 photoreduction over brookite-containing mixed-phase TiO_2 catalytic material. It is hypothesized that the molecules of interest will exhibit more favorable adsorption energies on the brookite TiO_2 (210) surface. Reasoning for this proposed hypothesis stems from the fact that brookite is orthorhombic in structure

and possesses longer Ti—O bond distances; thus, providing more surface area for direct adsorption or interaction with molecules. The key research questions of this study are:

- How do the adsorption energies and the charges of the molecules adsorbed on brookite TiO_2 (210) surfaces compare to those obtained on the anatase TiO_2 (101) surface?
- How does the state of the TiO_2 surfaces (neutral, negatively charged, positively charged and oxygen-deficient) affect charge transfer and adsorption capabilities?
- How do the theoretical vibrational frequencies of the molecules on TiO_2 compare to experimental data?

Answering such questions will assist in better understanding the intermediate reaction pathways associated with utilizing brookite-containing TiO_2 materials for CO_2 reduction to fuels.

CHAPTER 3: METHODOLOGY

3.1 Density Functional Theory Studies

In computational studies where the interaction of molecules with nanocomposites is being studied, cluster models or periodic slabs can be utilized to replicate the surface. In reference to computational work specific to the interaction of molecules with TiO_2 surfaces, cluster models are the most prevalent. It is imperative to note, however, that the periodic nature of the TiO_2 surface is neglected in cluster models. As a result, cluster models only provide an initial account of what type of interactions are taking place on the surface. Work published by He *et al*., Indrakanti *et al*., Wanbayor *et al*., and Nik *et al*. all entail the use of small TiO_2 clusters and periodic structures as a representation of the interacting surface.[56, 57, 66-69] For this study, the same methodology was employed in order to investigate the interaction of small molecules on the anatase TiO_2 (101) and brookite TiO_2 (210) surfaces.

A $Ti_7O_{27}H_{26}$ cluster model representing the anatase TiO_2 (101) surface was cleaved from the (101) plane of the anatase phase. All peripheral oxygens in the cluster were saturated with H atoms to terminate all dangling bonds. The same procedure was implemented to create the brookite TiO_2 (210) cluster model ($Ti_7O_{28}H_{28}$). The partially reduced or oxygen vacant (V_o) surfaces were modeled in both clusters by removing one top bridging O_{2c} atom. Negatively charged anatase TiO_2 (101) and brookite TiO_2 (210) surfaces were obtained by introducing an extra electron into the system and screening the hole - consequently modeling

the photoexcited electron. The positively charged anatase TiO_2 (101) and brookite TiO_2 (210) surfaces were obtained by introducing an extra hole into the system and screening the electron – consequently modeling photoexcited hole generation.

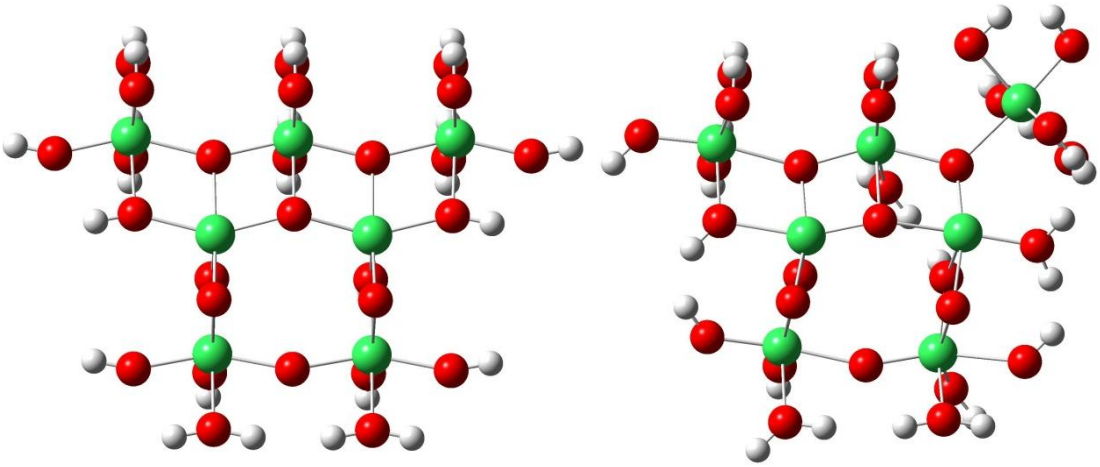

(a) (b)

Figure 3.1-1 TiO_2 cluster models: (a) anatase TiO_2 (101), (b) brookite TiO_2 (210); Ti atoms in green, O atoms in red, H atoms in white. (This notation is used throughout this document)

Using the Gaussian03 computational chemistry software package, density functional theory (DFT) calculations with the B3LYP functional were performed to investigate the adsorption behavior of CO, H_2O, and CH_4 gases on the neutral, negatively charged, positively charged, and oxygen-deficient brookite TiO_2 (210) and anatase TiO_2 (101) surfaces.[70] Optimizations of the individual species were performed first. Thereafter, the geometries of the various adsorbate-TiO_2 cluster configurations were optimized. All hydroxyl groups in the TiO_2 clusters were frozen during optimization to better represent the surface environment. The 6-31+G(2df,p) basis set used for the CO, H_2O, and CH_4 molecules and the five

surface O atoms in both the anatase TiO_2 (101) and brookite TiO_2 (210) clusters. The LanL2DZ basis set was used for the Ti, H, and all remaining O atoms in the cluster models. Natural bond orbital (NBO) charge analyses and vibrational frequency calculations for all adsorbate-TiO_2 cluster configurations were performed. Vibrational frequencies were scaled by a factor of 0.9652. The adsorption energies of each adsorbate were computed using the following equation:

$$\Delta \mathbf{E}_{\mathbf{adsorption}} = \mathbf{E}_{\mathbf{adsorbate\text{-}cluster}} - (\mathbf{E}_{\mathbf{adsorbate}} + \mathbf{E}_{\mathbf{cluster}})$$

Where **E** denotes the total energy of the individual or collective species (e.g. adsorbate, cluster, adsorbate-cluster) representing the system. In this study, two basis sets are utilized to compute the adsorption energies. The use of finite basis sets leads to basis set superposition errors (BSSE). To account for the BSSE of the complexes, a single-point energy calculation along with Boys and Bernardi counterpoise (CP) correction was performed for each complex.[71]

3.2 Adsorption-Desorption Experimental Studies

The adsorption and desorption behavior of H_2O vapor and CH_4 on nanocrystalline TiO_2 (Evonik P25) were investigated by diffuse reflection infrared Fourier transform spectroscopy (DRIFTS). DRIFTS is a powerful technique that exhibits high sensitivity for gaseous species on solid materials. Commonly used in experimental catalytic studies, DRIFTS is suitable in such a way that it can execute real-time identification of reactions occurring on a surface. For example, DRIFTS can detect end products and reaction intermediate species while a

reaction is taking place. The results from this experimental study serve not only as a comparison to the proposed theoretical work, but also as a means for addressing questions that are crucial to better understanding the photocatalytic reaction mechanisms.

The DRIFTS studies were performed on a Thermo Nicolet FTIR 6700 spectrometer (with OMNIC software) equipped with a Praying Mantis™ diffuse reflectance accessory. A 316 stainless steel high-temperature chamber (HVC, Harrick Scientific) was used as the reactor (Figure 3.2-1).

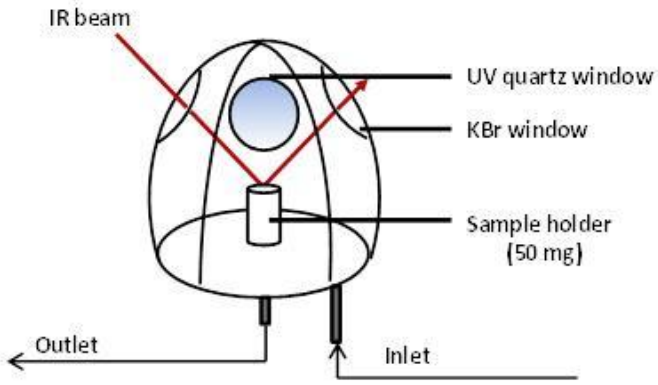

Figure 3.2-1 Schematic of DRIFTS reactor cell.

The H_2O adsorption-desorption experiments were carried out under STP conditions (20°C, 1 atm) in the DRIFTS HVC reactor. The Evonik P25 TiO_2 powder (~50 mg) was pretreated with a gas flow of ultra-high pure helium (99.999%, in-house) at a flowrate of 0.35 $L \cdot min^{-1}$ for 15 minutes. Ultra-high pure nitrogen (99.999%, in-house) was flowed through an impinger containing 0.35 L

of NanoPure filtered H_2O at a flowrate of 0.5 $L \cdot min^{-1}$. Following the 15 minute helium pretreatment, the inlet flow was switched to the saturated nitrogen flow – exposing the TiO_2 powder sample to H_2O vapor. After 21 minutes, a switch in inlet flow from H_2O vapor to helium ensued. The purpose of this procedure was to purge the TiO_2 sample and remove any residual H_2O species on the surface. The two sequential steps of exposing the TiO_2 sample to H_2O vapor (at 0.5 $L \cdot min^{-1}$) then to a helium purge (0.35 $L \cdot min^{-1}$) constitutes as one adsorption-desorption cycle. Accordingly, these two steps were implemented over a duration of 110 minutes to yield three adsorption-desorption cycles. The flowrates throughout this experiment were kept constant.

As in the H_2O adsorption-desorption experiments, the CH_4 adsorption-desorption experiments were carried out under STP conditions in the DRIFTS HVC reactor. Evonik P25 TiO_2 powder (~50 mg) was pretreated with a gas flow of ultra-high pure helium (99.999%, in-house) at a flowrate of 0.12 $L \cdot min^{-1}$ for 15 minutes. Following the 15 minute helium pretreatment of the sample, the inlet flow was switched to pure CH_4 gas (99.99%, Sigma-Aldrich) at a flowrate of 0.24 $L \cdot min^{-1}$. After 21 minutes, a switch in inlet flow from CH_4 gas to helium ensued in order to desorb all CH_4 contents on the TiO_2 surface. The two sequential steps of exposing the TiO_2 sample to CH_4 gas (at 0.24 $L \cdot min^{-1}$) then to a helium purge (0.12 $L \cdot min^{-1}$) were implemented over a duration of 92 minutes to yield three adsorption-desorption cycles. All flowrates throughout this experiment were kept constant.

CHAPTER 4: RESULTS

4.1 CO on Anatase and Brookite Cluster Models

The optimized geometries of CO adsorbed on neutral, negatively charged, and oxygen deficient anatase TiO_2 clusters are shown in Figures 4.1-1, 4.1-2, and 4.1-3, respectively. The configurations for CO adsorbed on neutral, negatively charged, and oxygen deficient brookite TiO_2 clusters are shown in Figures 4.1-4, 4.1-5, and 4.1-6, respectively. The adsorption energies (uncorrected and BSSE corrected) and NBO charges of CO are displayed in Tables 4.1-7 and 4.1-8. The C—Ti distances (in Å) and IR frequencies (in cm^{-1}) with respect to each configuration are shown in Tables 4.1-9 and 4.1-10.

Two configurations were obtained for CO on the neutral anatase TiO_2 (101) cluster surface (configurations 1A and 1B). In the 1A configuration, the CO molecule is vertically positioned above the cluster model's surface with the C atom interacting with the Ti_{5c} site. The 1B configuration entails the CO molecule vertically positioned above the cluster model's surface with the O atom interacting with the Ti_{5c} site. For the negatively charged system, these same CO orientations (configurations 2A and 2B) were obtained. Distinct configurations (3A and 3B) for CO on the oxygen vacant anatase TiO_2 (101) cluster surface were obtained. In the 3A configuration, the CO molecule is diagonally positioned above the oxygen-vacant site. This configuration also shows the C atom interacts with the Ti_{5c} reactive site. Likewise, the 3B configuration comprises of the CO

molecule oriented above the oxygen-vacant site, but with C atom interacting with the Ti_{6c} reactive site.

Four configurations were obtained for CO on the neutral brookite TiO_2 (210) cluster surface (configurations 1A, 1B, 1C, and 1D). In the 1A configuration, the CO molecule is vertically positioned above the cluster model's surface with the C atom interacting with the Ti_{5c} site. The 1B configuration entails the CO molecule vertically positioned above the cluster model's surface with the O atom interacting with the Ti_{5c} site. In configuration 1C, the CO molecule is vertically positioned above the cluster model's surface with the C atom interacting with the second Ti_{5c} site (which is closest to the dangling Ti_{6c} site). Configuration 1D entails the same binding site as that of configuration 1C; wherein the O atom of the CO molecule interacts with the Ti_{5c} site. For the negatively charged system, these same CO orientations (configurations 2A, 2B, 2C and 2D) were obtained. Distinct configurations (3A and 3B) for CO on the oxygen vacant brookite TiO_2 (101) cluster surface were obtained. In the 3A configuration, the CO molecule is diagonally positioned above the oxygen-vacant site. This configuration also shows the C atom interacts with the Ti_{5c} reactive site. Likewise, the 3B configuration comprises of the CO molecule oriented above the oxygen-vacant site, but with C atom interacting with the Ti_{6c} reactive site.

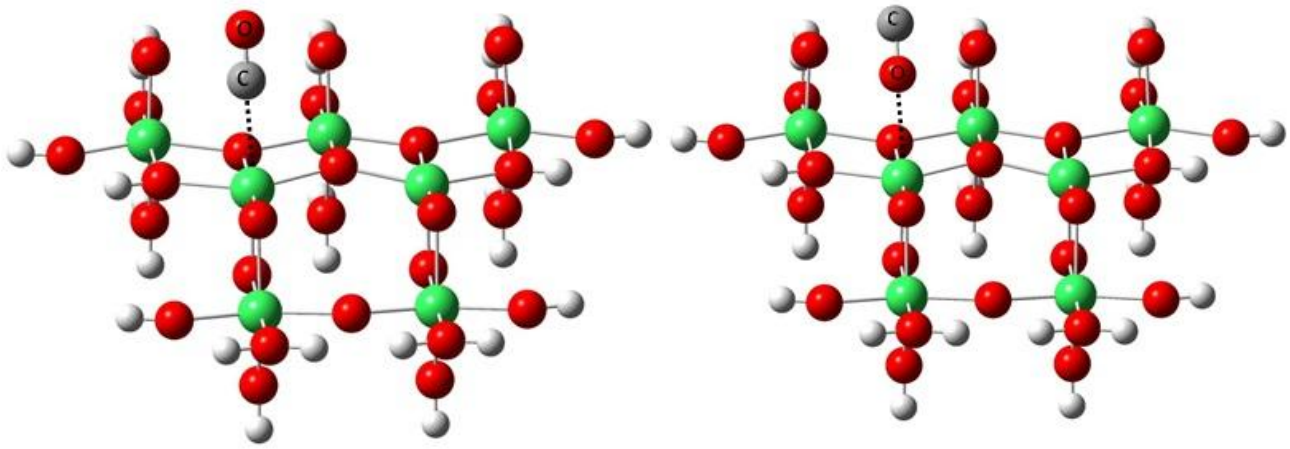

(1A) **(1B)**

354

Figure 4.1-1 Adsorption configurations of CO adsorbed on the anatase TiO_2 (101) surface: (1A) and (1B) CO on neutral surface.

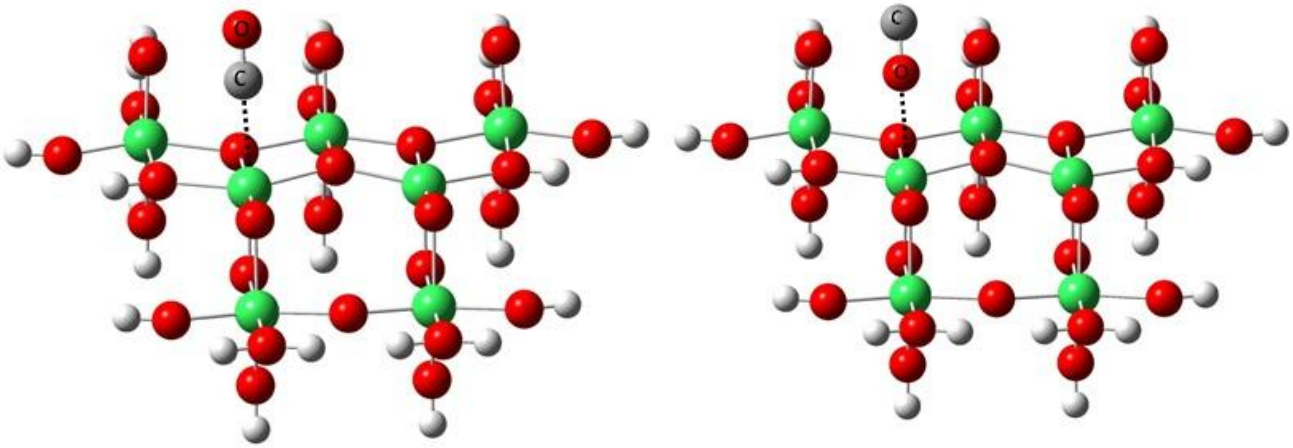

(2A) **(2B)**

Figure 4.1-2 Adsorption configurations of CO adsorbed on the anatase TiO_2 (101) surface: (2A) and (2B) CO on negatively charged surface.

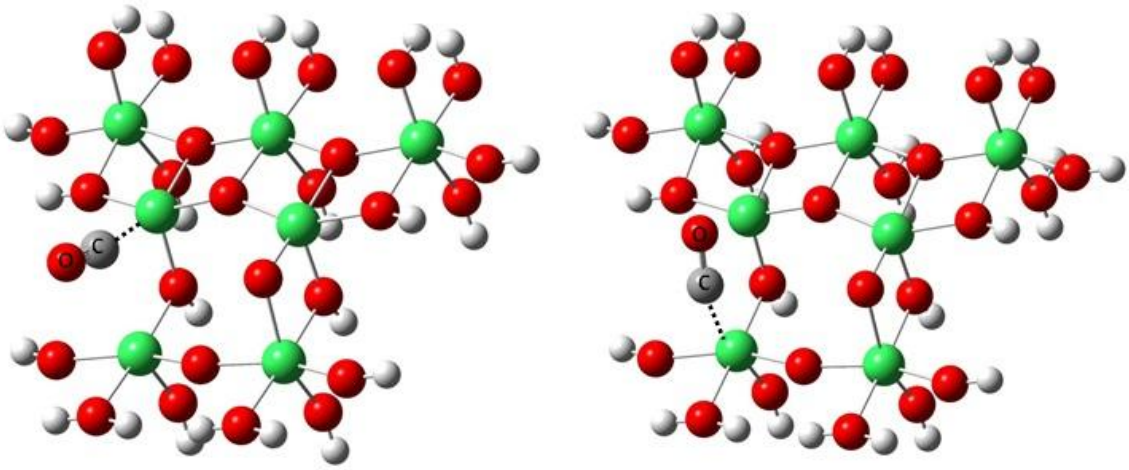

(3A) **(3B)**

Figure 4.1-3 Adsorption configurations of CO adsorbed on the anatase TiO_2 (101) surface: (3A) and (3B) CO on V_o surface.

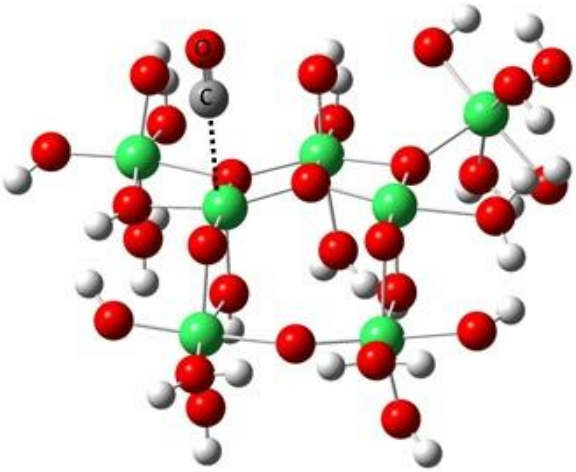

(1A)

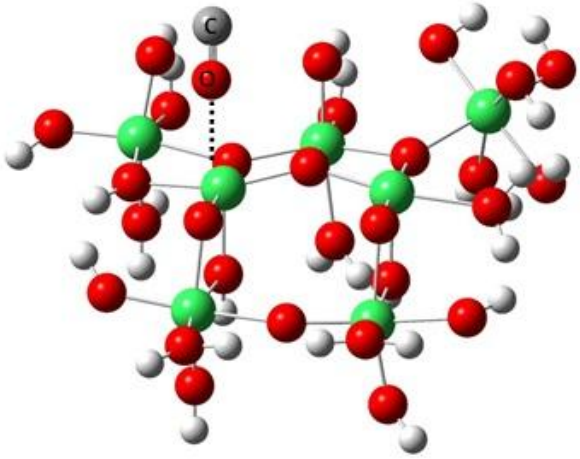

(1B)

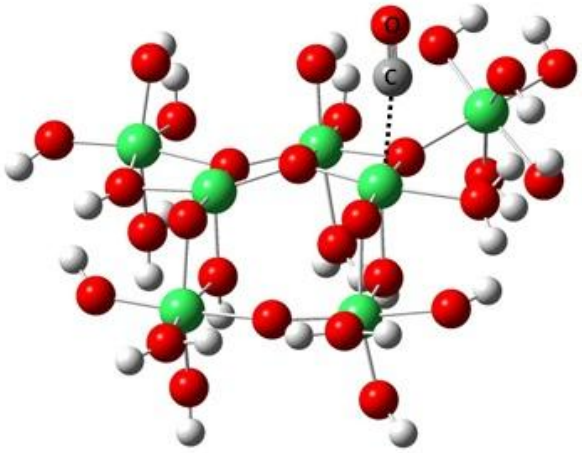

(1C)

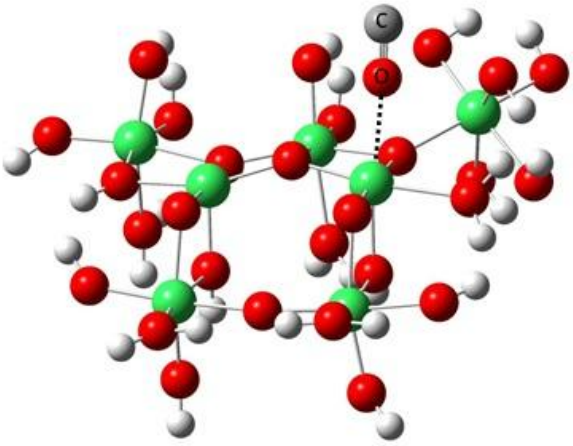

(1D)

Figure 4.1-4 Adsorption configurations of CO adsorbed on the brookite TiO_2 (210) surface: (1A), (1B), (1C) and (1D) CO on neutral surface.

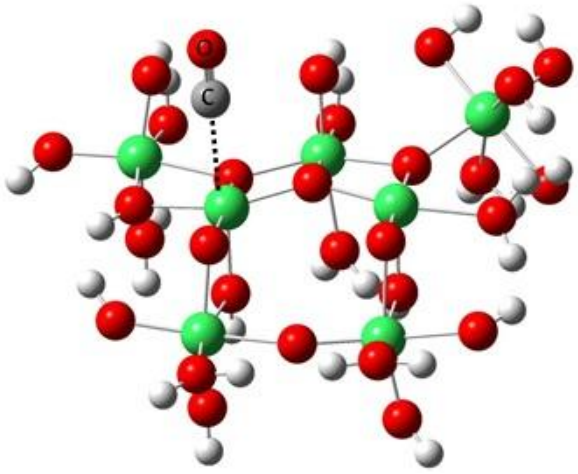

(2A)

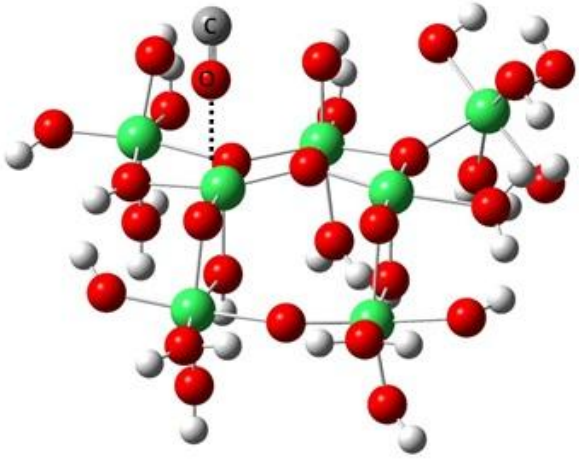

(2B)

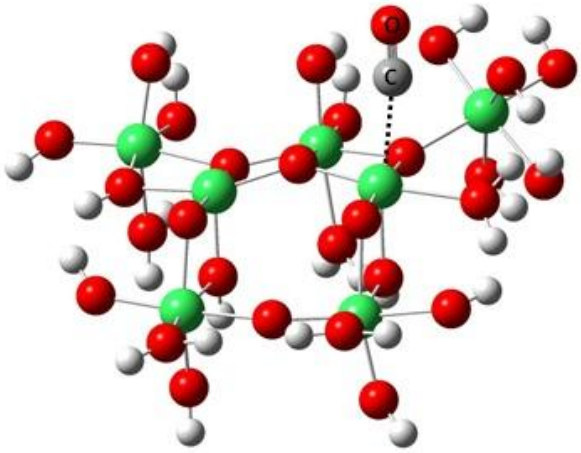

(2C)

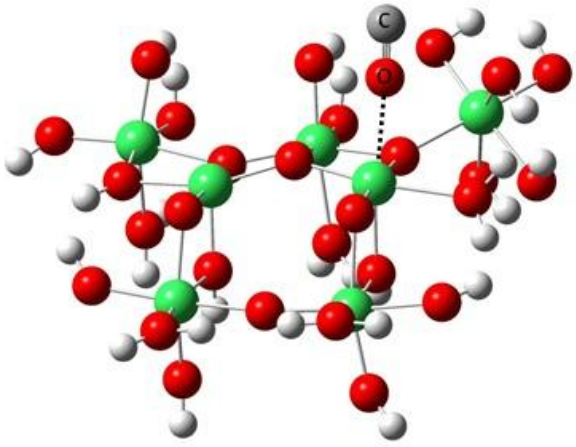

(2D)

Figure 4.1-5 Adsorption configurations of CO adsorbed on the brookite TiO_2 (210) surface: (2A), (2B), (2C) and (2D) CO on negatively charged surface.

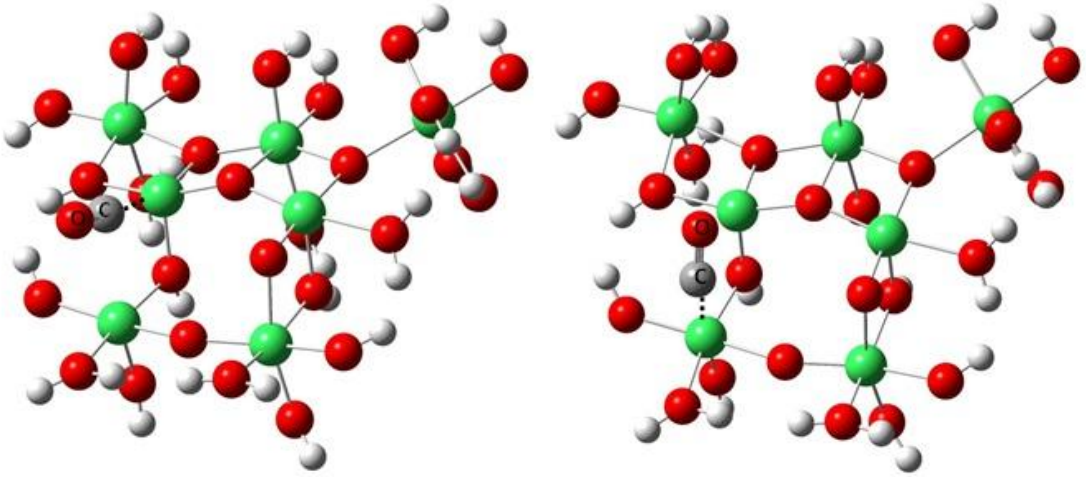

(3A) **(3B)**

Figure 4.1-6 Adsorption configurations of CO adsorbed on the brookite TiO_2 (210) surface: (3A) and (3B) CO on V_o surface.

Table 4.1-7 ΔE_{ads} (in eV) and NBO charge of CO on anatase (101)

surface	anatase (101)								
state	neutral (configuration 1)			negatively-charged (configuration 2)			oxygen-deficient (configuration 3)		
Configuration	ΔE_{ads}	Charge	ΔE_{ads}^{BSSE}	ΔE_{ads}	Charge	ΔE_{ads}^{BSSE}	ΔE_{ads}	Charge	ΔE_{ads}^{BSSE}
A	-0.372	0.338	-0.379	-0.300	0.315	-0.498	-1.634	-0.060	-1.871
B	-0.145	0.121	-0.133	-0.105	0.093	-0.302	-1.811	0.046	-1.839

Table 4.1-8 ΔE_{ads} (in eV) and NBO charge of CO on brookite (210)

surface	brookite (210)								
state	neutral (configuration 1)			negatively-charged (configuration 2)			oxygen-deficient (configuration 3)		
Configuration	ΔE_{ads}	Charge	ΔE_{ads}^{BSSE}	ΔE_{ads}	Charge	ΔE_{ads}^{BSSE}	ΔE_{ads}	Charge	ΔE_{ads}^{BSSE}
A	-0.454	0.357	-0.460	-0.378	0.336	-0.582	-1.550	-0.058	-1.772
B	-0.193	0.147	-0.180	-0.129	0.124	-0.231	-1.600	0.052	-1.611
C	-0.530	0.349	-0.600	-0.613	0.276	-0.825	-	-	-
D	-0.213	0.152	-0.230	-0.202	0.121	-0.372	-	-	-

Table 4.1-9 Vibrational frequency (cm^{-1}) and C—Ti distance (Å) of CO on anatase (101) and brookite (210)

State and Configuration	v_1 (cm^{-1})	C-Ti (Å)
Anatase Neutral		
1A	2190	2.43
Brookite Neutral		
1A	2195	2.43
1A	2194	2.39
Brookite Negative		
2A	2169	2.43
2C	2061	2.21
Brookite Vo		
3A	1651	2.14
3B	1907	2.07

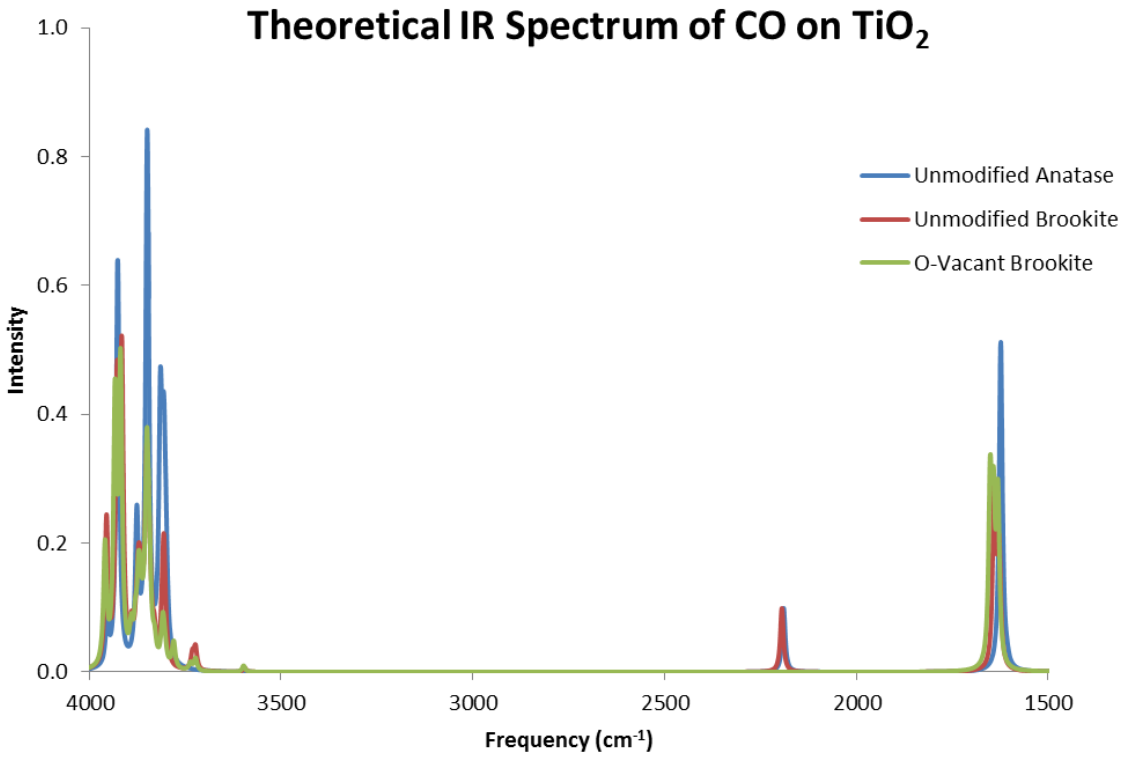

Figure 4.1-10 Theoretical IR spectra of CO on anatase (101) and brookite (210) surfaces.

4.2 H_2O on Anatase and Brookite Cluster Models

The optimized geometries of H_2O adsorbed on neutral, negatively charged, positively charge, and oxygen deficient anatase TiO_2 clusters are shown in Figures 4.2-1, 4.2-2, 4.2-3, and 4.2-4, respectively. The configurations for H_2O adsorbed on neutral, negatively charged, positively charged, and oxygen deficient brookite TiO_2 clusters are shown in Figures 4.2-5, 4.2-6, 4.2-7, and 4.2-8, respectively. The adsorption energies (uncorrected and BSSE corrected) and NBO charges of H_2O are displayed in Tables 4.2-9 and 4.2-10. The O—Ti distances (in

Å) and IR frequencies (in cm^{-1}) with respect to each configuration are shown in Tables 4.2-11 and 4.2-12. One configuration was obtained for H_2O on the neutral anatase TiO_2 (101) cluster surface (configuration 1A). In the 1A configuration, the O atom in the H_2O molecule is positioned directly above the Ti_{5c} site. For the negatively and positively charged systems, configurations 2A and 3A were obtained. Distinct configurations (4A and 4B) for H_2O on the oxygen vacant anatase TiO_2 (101) cluster surface were obtained. In both configurations, the O atom in the H_2O molecule is positioned above the oxygen-vacant site. Two configurations were obtained for H_2O on the neutral brookite TiO_2 (210) cluster surface (configurations 1A and 1B). In configuration 1A, the O atom in the H_2O molecule is positioned directly above the Ti_{5c} site. The 1B configuration entails the H_2O molecule vertically positioned above the cluster model; wherein the O atom interacts with the second Ti_{5c} site (which is closest to the dangling Ti_{6c} site). For the negatively and positively charged systems, configurations 2A, 2B, 3A, and 3B were obtained. One distinct configuration (4A) for H_2O on the oxygen vacant brookite TiO_2 (101) cluster surface was obtained. This configuration also shows the O atom positioned over the oxygen vacant site.

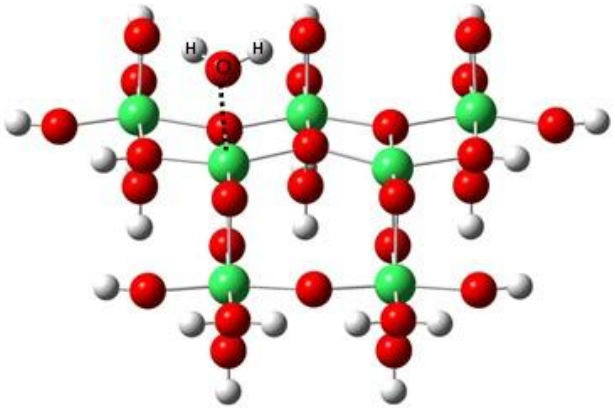

(1A)

Figure 4.2-1 Adsorption configuration of H_2O adsorbed on the anatase TiO_2 (101) surface: (1A) H_2O on neutral surface.

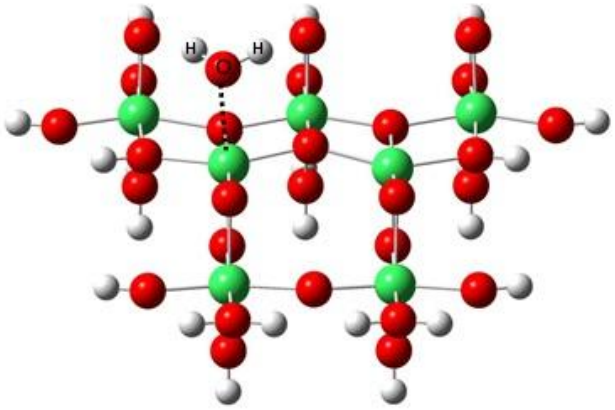

(2A)

Figure 4.2-2 Adsorption configuration of H_2O adsorbed on the anatase TiO_2 (101) surface: (2A) H_2O on negatively charged surface.

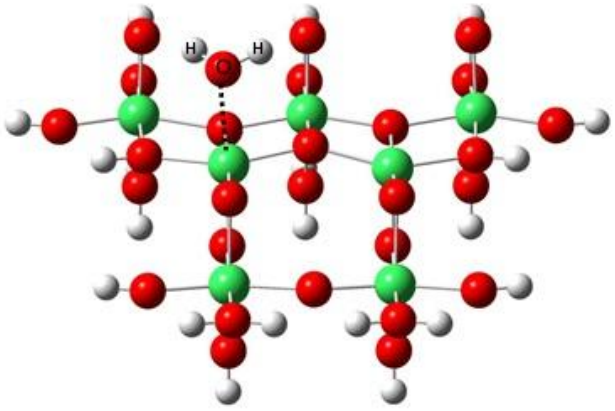

(3A)

Figure 4.2-3 Adsorption configuration of H_2O adsorbed on the anatase TiO_2 (101) surface: (3A) H_2O on positively charged surface.

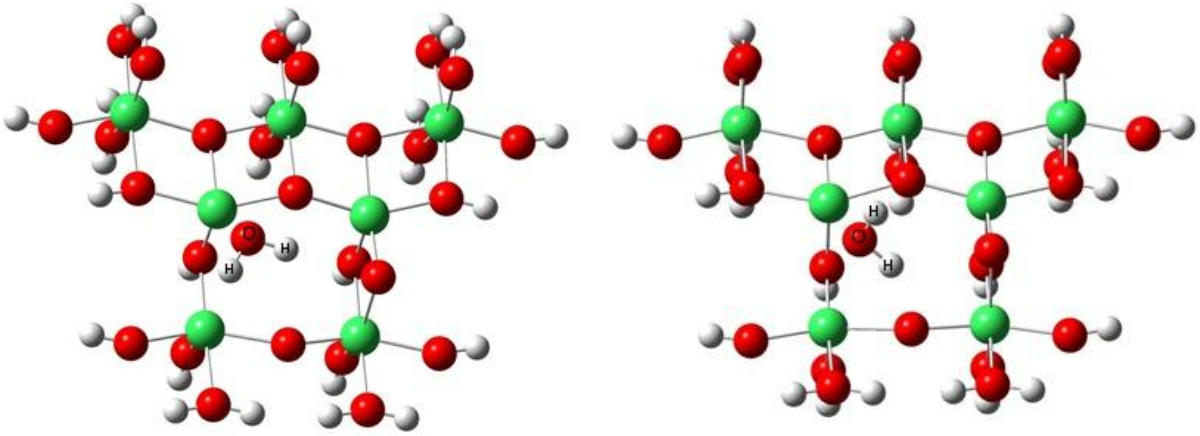

(4A) **(4B)**

Figure 4.2-4 Adsorption configurations of H_2O adsorbed on the anatase TiO_2 (101) surface: (4A) and (4B) H_2O on V_o surface.

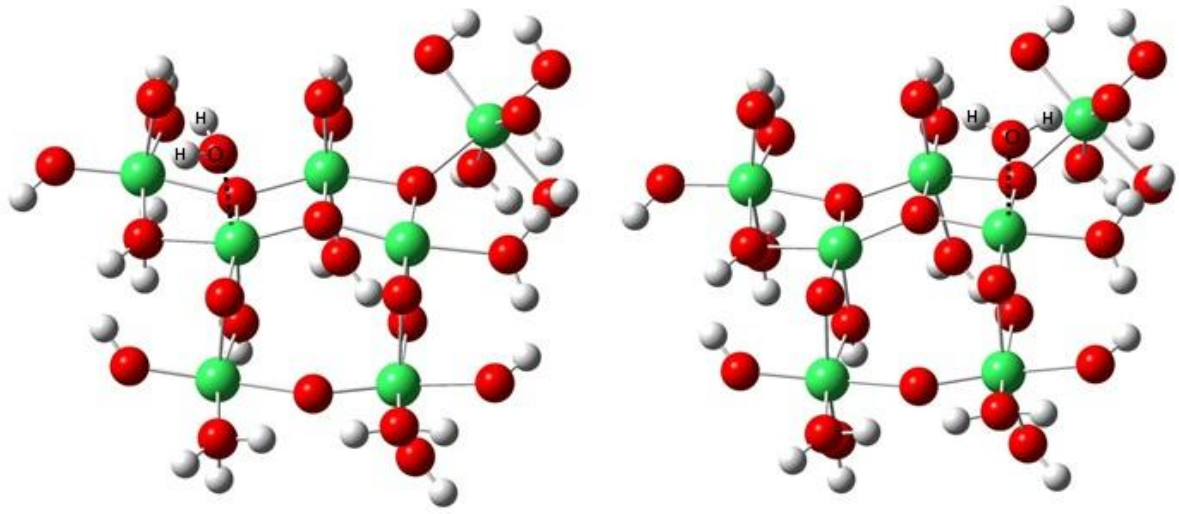

(1A) **(1B)**

Figure 4.2-5 Adsorption configurations of H_2O adsorbed on the brookite TiO_2 (210) surface: (1A) and (1B) H_2O on neutral surface.

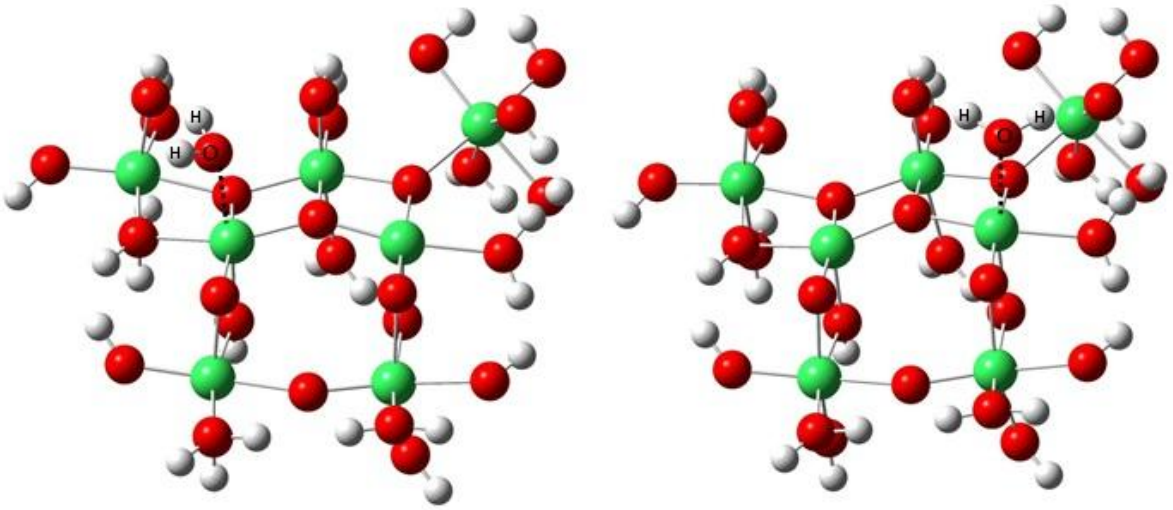

(2A) **(2B)**

Figure 4.2-6 Adsorption configurations of H_2O adsorbed on the brookite TiO_2 (210) surface: (2A) and (2B) H_2O on negatively charged surface.

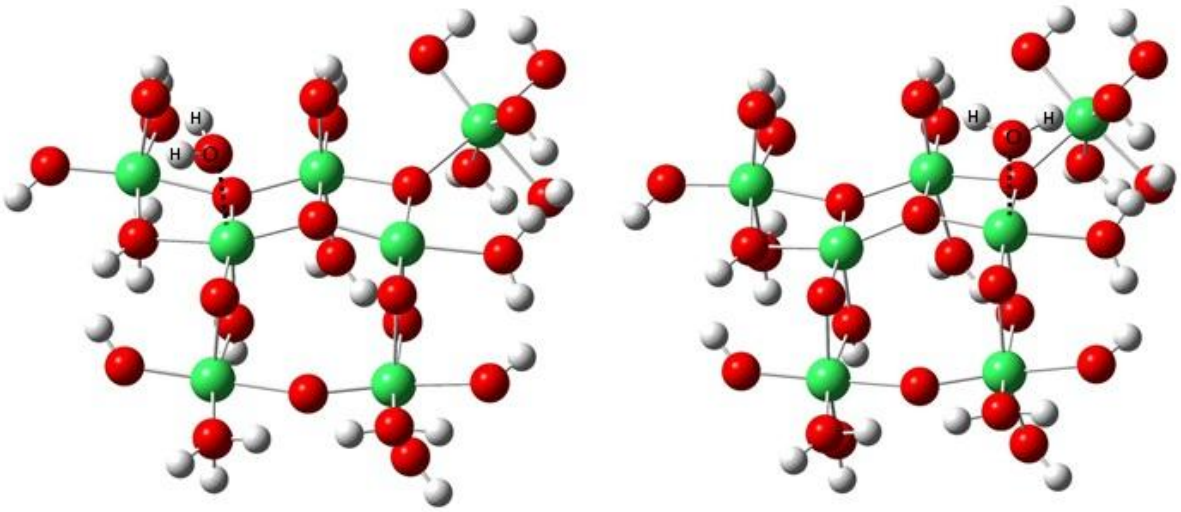

(3A) **(3B)**

Figure 4.2-7 Adsorption configurations of H_2O adsorbed on the brookite TiO_2 (210) surface: (3A) and (3B) H_2O on positively charged surface.

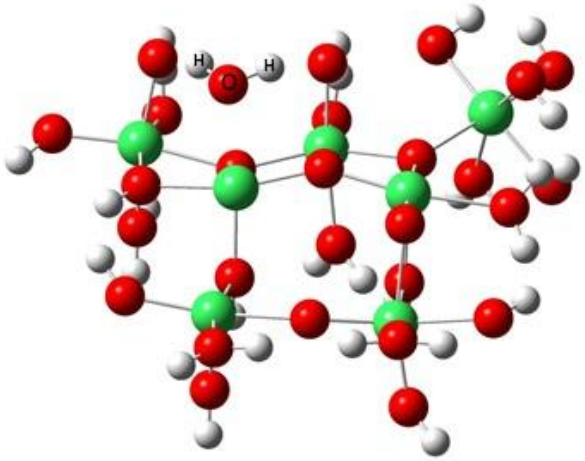

(4A)

Figure 4.2-8 Adsorption configuration of H_2O adsorbed on the brookite TiO_2 (210) surface: (4A) H_2O on V_o surface.

Table 4.2-9 ΔE_{ads} (in eV) and NBO charge of H_2O on anatase (101)

surface	anatase (101)											
state	neutral (configuration 1)			negatively-charged (configuration 2)			positively-charged (configuration 3)		oxygen-deficient (configuration 4)			
Configuration	ΔE_{ads}	Charge	ΔE_{ads}^{BSSE}	ΔE_{ads}	Charge	ΔE_{ads}^{BSSE}	ΔE_{ads}	Charge	ΔE_{ads}	Charge	ΔE_{ads}^{BSSE}	
A	-1.020	0.211	-1.145	-0.925	0.185	-1.196	-1.155	0.233	-0.996	0.167	-1.130	
B	-	-	-	-	-	-	-	-	-0.927	0.182	-0.955	

Table 4.2-10 ΔE_{ads} (in eV) and NBO charge of H_2O on brookite (210)

surface	brookite (210)											
state	neutral (configuration 1)			negatively-charged (configuration2)			positively-charged (configuration3)		oxygen-deficient (configuration4)			
Configuration	ΔE_{ads}	Charge	ΔE_{ads}^{BSSE}	ΔE_{ads}	Charge	ΔE_{ads}^{BSSE}	ΔE_{ads}	Charge	ΔE_{ads}	Charge	ΔE_{ads}^{BSSE}	
A	-1.161	0.220	-1.320	-1.230	0.197	-1.489	-1.486	0.234	-1.376	0.176	-1.449	
B	-1.539	0.199	-1.763	-1.319	0.153	-1.516	-1.616	0.215	-	-	-	

Table 4.2-11 Vibrational frequency (cm^{-1}) and O—Ti distance (Å) of H_2O on anatase (101) and brookite (210)

State and Configuration	v_1 (cm^{-1})	v_2 (cm^{-1})	v_3 (cm^{-1})	C-Ti (Å)
Anatase Neutral				
1A	3464	3615	1609	2.23
Brookite Neutral				
1A	3167	3718	1594	2.15
1B	2925	3460	1671	2.12
Brookite Negative				
2A	3168	3502	1636	2.20
2B	3198	3418	1659	2.20
Brookite Vo				
4A	3204	3557	1633	2.19

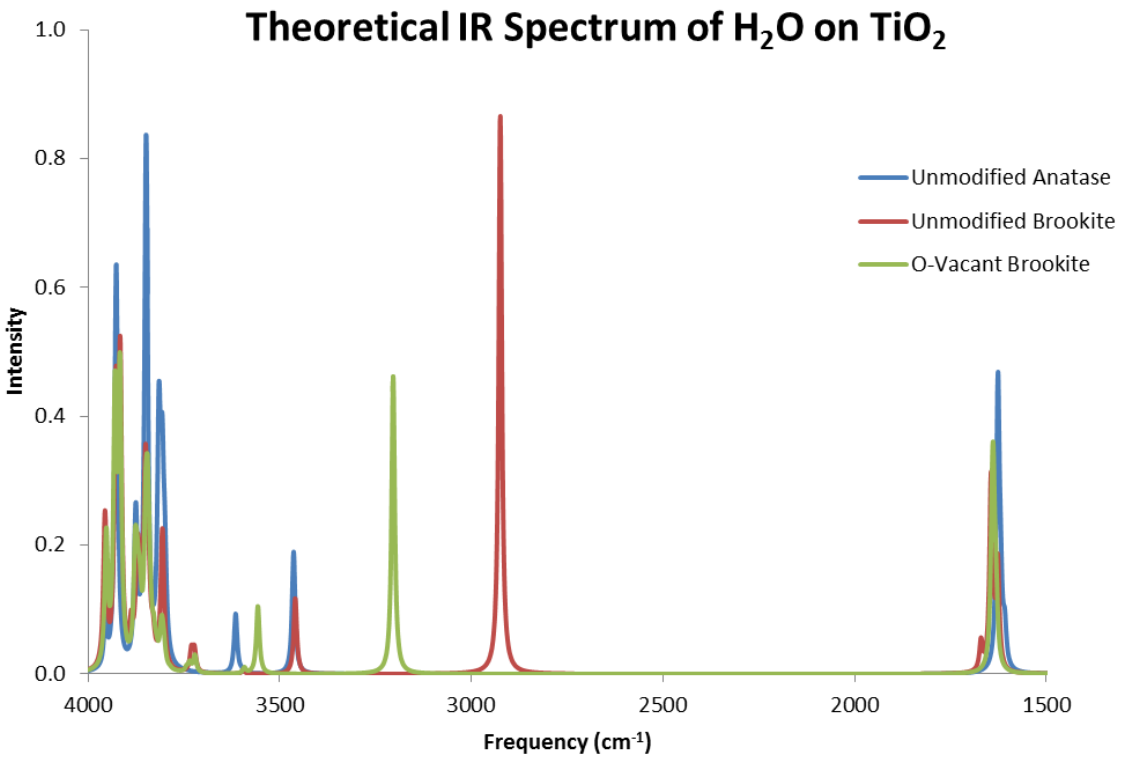

Figure 4.2-12 Theoretical IR spectra of H_2O on anatase (101) and brookite (210) surfaces.

4.3 CH_4 on Anatase and Brookite Cluster Models

The optimized geometries of CH_4 adsorbed on neutral, negatively charged, positively charge, and oxygen deficient anatase TiO_2 clusters are shown in Figures 4.3-1, 4.3-2, 4.3-3, and 4.3-4, respectively. The optimized geometries of CH_4 adsorbed on neutral, negatively charged, positively charge, and oxygen deficient brookite TiO_2 clusters are shown in Figures 4.3-5, 4.3-6, 4.3-7, and 4.3-8, respectively. The adsorption energies (uncorrected and BSSE corrected) and NBO charges of CH_4 are displayed in Tables 4.3-9 and 4.3-10. The C—Ti distances (in Å) and IR frequencies (in cm^{-1}) with respect to each configuration are shown in Tables 4.3-11 and 4.3-12. One configuration was obtained for CH_4 on the neutral anatase TiO_2 (101) cluster surface (configuration 1A). In the 1A configuration, the C atom in the CH_4 molecule is positioned directly above the Ti_{5c} site. For the negatively and positively charged systems, configurations 2A and 3A were obtained. One distinct configuration, 4A, for CH_4 on the oxygen vacant anatase TiO_2 (101) cluster surface was obtained. In this configuration, an H atom in the CH_4 molecule is positioned above the oxygen-vacant site. Two configurations were obtained for CH_4 on the neutral brookite TiO_2 (210) cluster surface (configurations 1A and 1B). In configuration 1A, the C atom in the CH_4 molecule is positioned directly above the Ti_{5c} site. The 1B configuration entails the CH_4 molecule vertically positioned above the cluster model; wherein the C atom interacts with the second Ti_{5c} site (which is closest to the dangling Ti_{6c} site). For the negatively and positively charged systems 2A, 2B, 3A, and 3B were obtained. One distinct configuration (4A) for CH_4 on the oxygen vacant brookite

TiO_2 (101) cluster surface was obtained. This configuration also shows an H atom positioned over the oxygen vacant site.

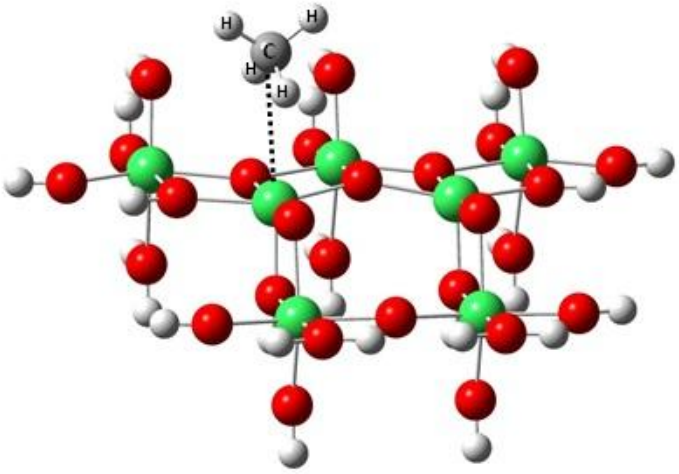

(1A)

Figure 4.3-1 Adsorption configuration of CH_4 adsorbed on the anatase TiO_2 (101) surface: (1A) CH_4 on neutral surface.

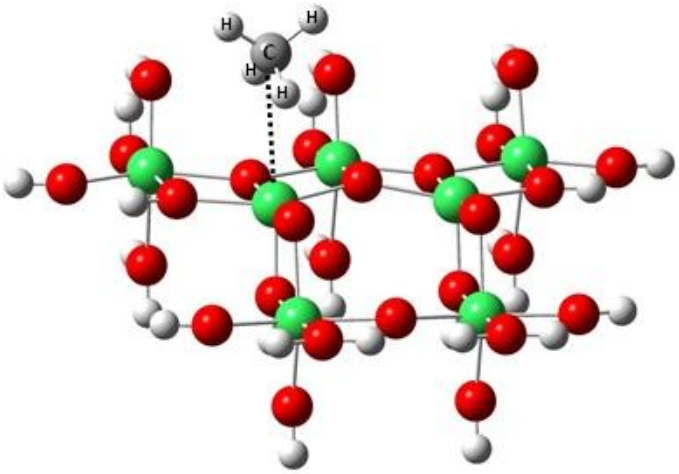

(1A)

Figure 4.3-2 Adsorption configuration of CH_4 adsorbed on the anatase TiO_2 (101) surface: (1A) CH_4 on negatively charged surface.

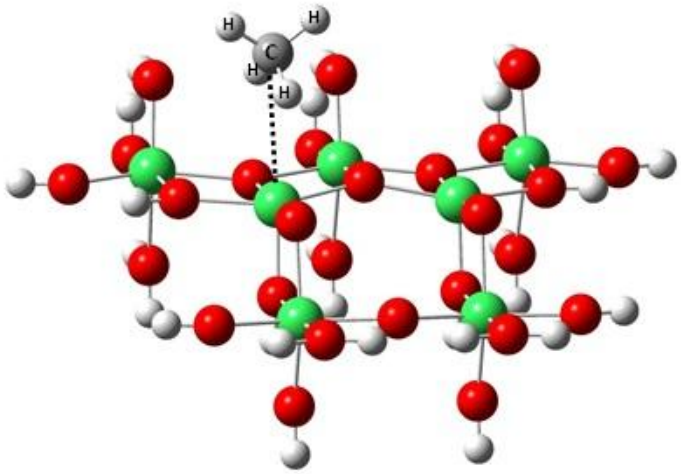

(3A)

Figure 4.3-3 Adsorption configuration of CH_4 adsorbed on the anatase TiO_2 (101) surface: (3A) CH_4 on positively charged surface.

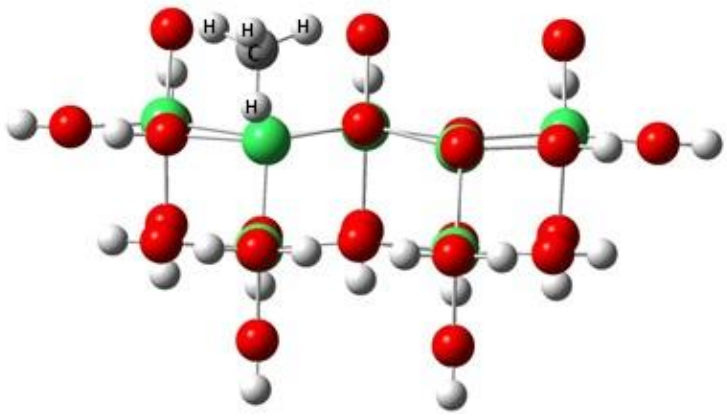

(4A)

Figure 4.3-4 Adsorption configuration of CH_4 adsorbed on the anatase TiO_2 (101) surface: (4A) CH_4 on V_o surface.

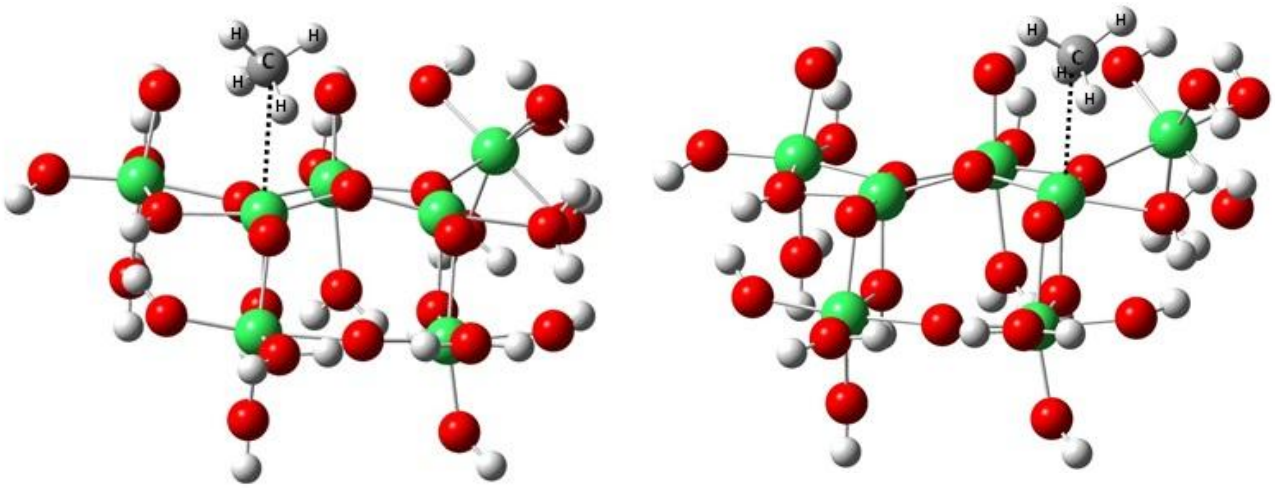

(1A) **(1B)**

Figure 4.3-5 Adsorption configurations of CH_4 adsorbed on the brookite TiO_2 (210) surface: (1A) and (1B) CH_4 on neutral surface.

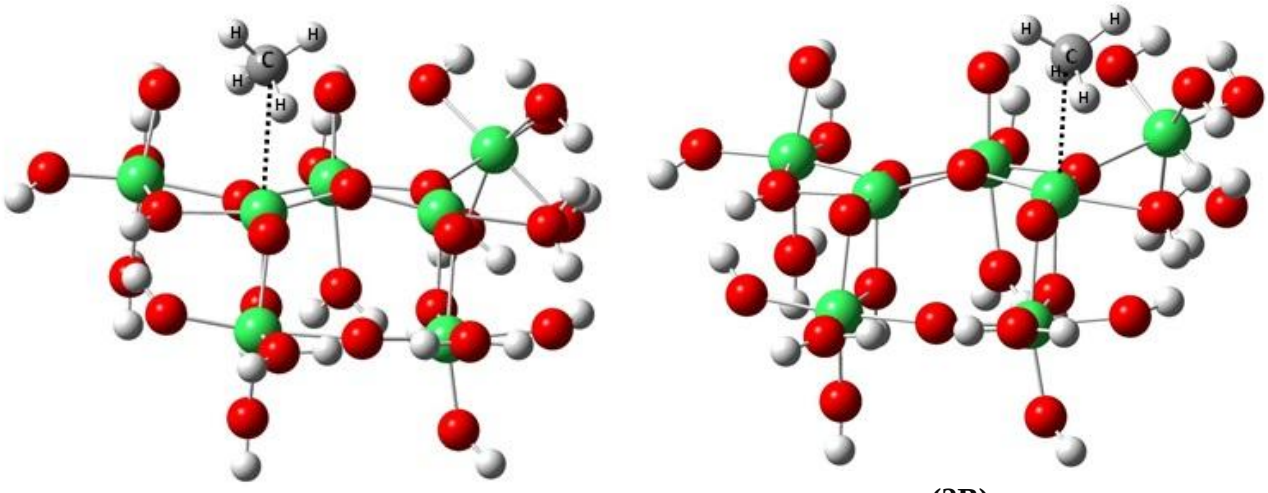

(2A) **(2B)**

Figure 4.3-6 Adsorption configurations of CH_4 adsorbed on the brookite TiO_2 (210) surface: (2A) and (2B) CH_4 on negatively charged surface.

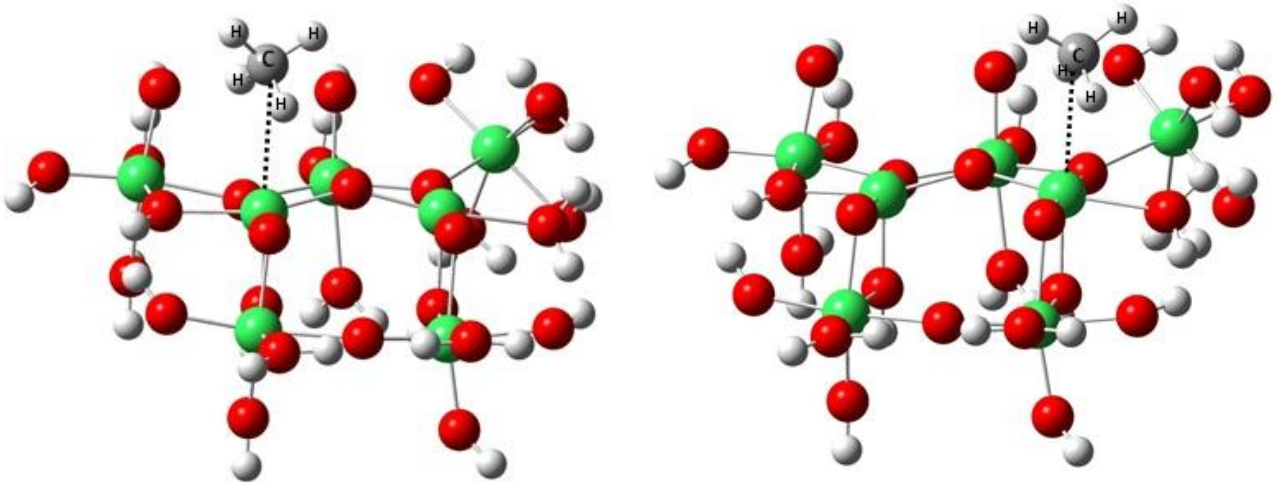

(3A) **(3B)**

Figure 4.3-7 Adsorption configurations of CH_4 adsorbed on the brookite TiO_2 (210) surface: (3A) and (3B) CH_4 on positively charged surface.

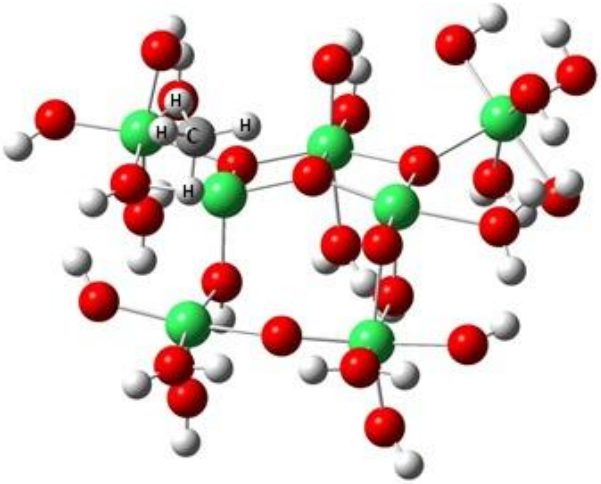

(4A)

Figure 4.3-8 Adsorption configuration of CH_4 adsorbed on the brookite TiO_2 (210) surface: (4A) CH_4 on V_o surface.

Table 4.3-9 ΔE_{ads} (in eV; uncorrected and corrected) and NBO charge of CH_4 on anatase (101)

surface	anatase (101)										
state	neutral (configuration 1)			negatively-charged (configuration 2)			positively-charged (configuration 3)		oxygen-deficient (configuration 4)		
Configuration	ΔE_{ads}	Charge	ΔE_{ads}^{BSSE}	ΔE_{ads}	Charge	ΔE_{ads}^{BSSE}	ΔE_{ads}	Charge	ΔE_{ads}	Charge	ΔE_{ads}^{BSSE}
A	-0.066	0.066	-0.033	-0.055	0.007	-0.281	-0.124	0.103	-0.324	0.108	-0.372

Table 4.3-10 ΔE_{ads} (in eV; uncorrected and corrected) and NBO charge of CH_4 on brookite (101)

surface	brookite (210)										
state	neutral (configuration 1)			negatively-charged (configuration 2)			positively-charged (configuration 3)		oxygen-deficient (configuration 4)		
Configuration	ΔE_{ads}	Charge	ΔE_{ads}^{BSSE}	ΔE_{ads}	Charge	ΔE_{ads}^{BSSE}	ΔE_{ads}	Charge	ΔE_{ads}	Charge	ΔE_{ads}^{BSSE}
A	-0.091	0.083	-0.032	-0.056	0.028	-0.300	-0.149	0.130	-0.300	0.124	-0.266
B	-0.126	0.112	-0.108	-0.120	0.070	-0.337	-0.223	0.144	-	-	-

Table 4.3-11 Vibrational frequency (cm^{-1}) and C—Ti distance (Å) of CH_4 on anatase (101) and brookite (210)

State and Configuration	v_1 (cm^{-1})	v_2 (cm^{-1})	v_3 (cm^{-1})	v_4 (cm^{-1})	C-Ti (Å)
Anatase Neutral					
A	2911	1492, 1518	3013, 3024, 3044	1248, 1254, 1302, 1320	3.11
Brookite Neutral					
A	2904	1494, 1519	3008, 3012, 3052	1245, 1299, 1328	3.03
B	2893	1485, 1523	2994, 3019, 3063	1222, 1301, 1336	2.87
Brookite Negative					
A	2909	1501, 1514	3002, 3024, 3040	1276, 1289, 1315	3.40
B	2887	1509, 1520	2987, 2997, 3051	1267, 1303, 1324	2.91
Brookite Vo					
A	2950	1474, 1563	3019, 3066	1255, 1289, 1344	2.57

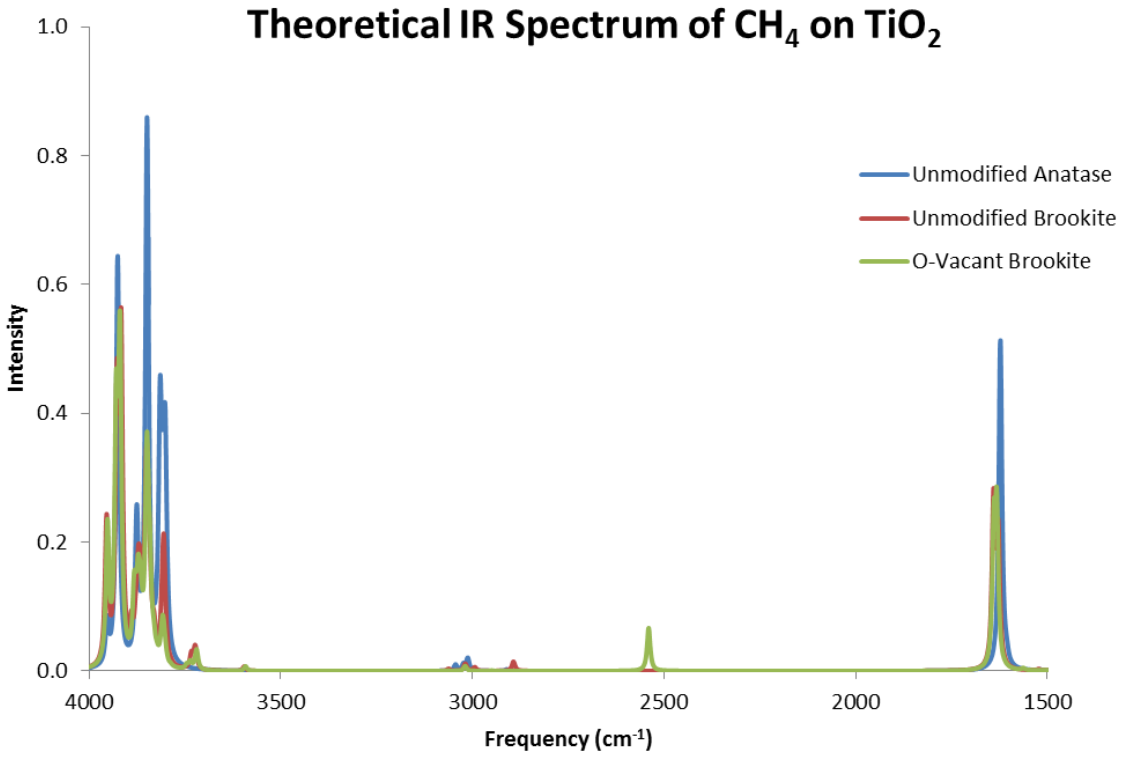

Figure 4.3-12 Theoretical IR spectra of CH_4 on anatase (101) and brookite (210) surfaces.

4.4 Experimental Adsorption-Desorption Plots

According to literature, the H_2O and CH_4 molecules can be characterized by three and four vibrational modes, respectively (shown in Tables 4.4-1 and 4.4-2) An adsorption-desorption plot of H_2O on Evonik P25 TiO_2 was constructed by measuring the intensity (IR absorbance) of features characteristic to O—H bond bending (v_3=1652 cm^{-1}) over a period of 110 minutes. The adsorption-desorption plot of CH_4 on P25 TiO_2 was constructed utilizing the same methodology, but for features characteristic to asymmetric stretching of C—H bonds (v_3=3016 cm^{-1}).

Table 4.4-1 Vibrational modes of H_2O molecule[72]

Mode	Description	Frequency (cm^{-1})
v_1	symmetrical stretching	3650
v_2	asymmetrical stretching	3750
v_3	O—H bond bending	1600

Table 4.4-2 Vibrational modes of CH_4 molecule[73]

Mode	Description	Frequency (cm^{-1})
v_1	symmetrical C—H stretching	2914
v_2	asymmetrical CH_3 deformation	1526
v_3	asymmetrical C—H stretching	3020
v_4	symmetrical CH_3 deformation	1305

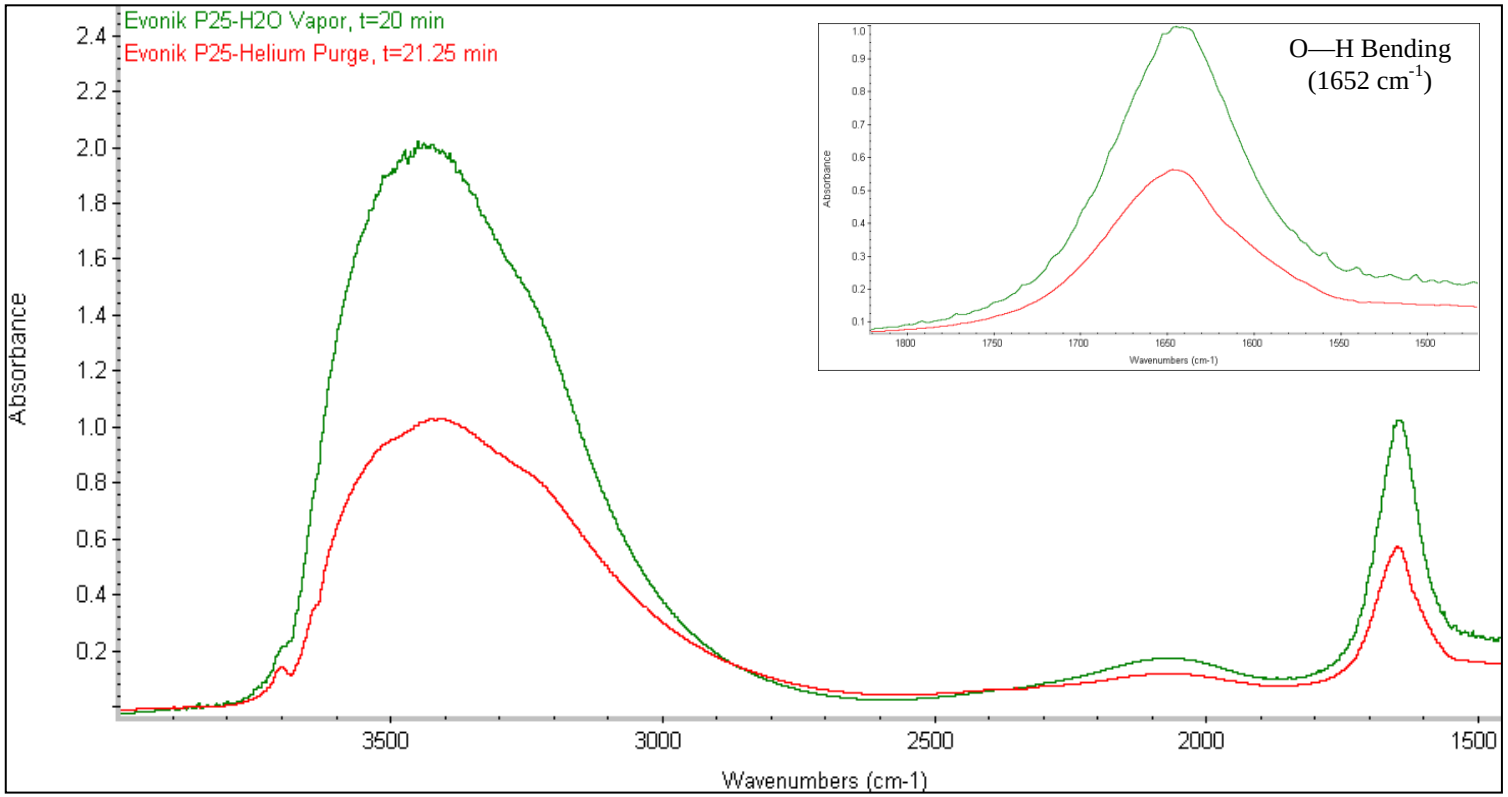

Figure 4.4-3 Experimental IR spectra of H_2O adsorption-desorption on Evonik P25 TiO_2 with respect to time. (Characteristic feature of O-H bending is shown in inset figure).

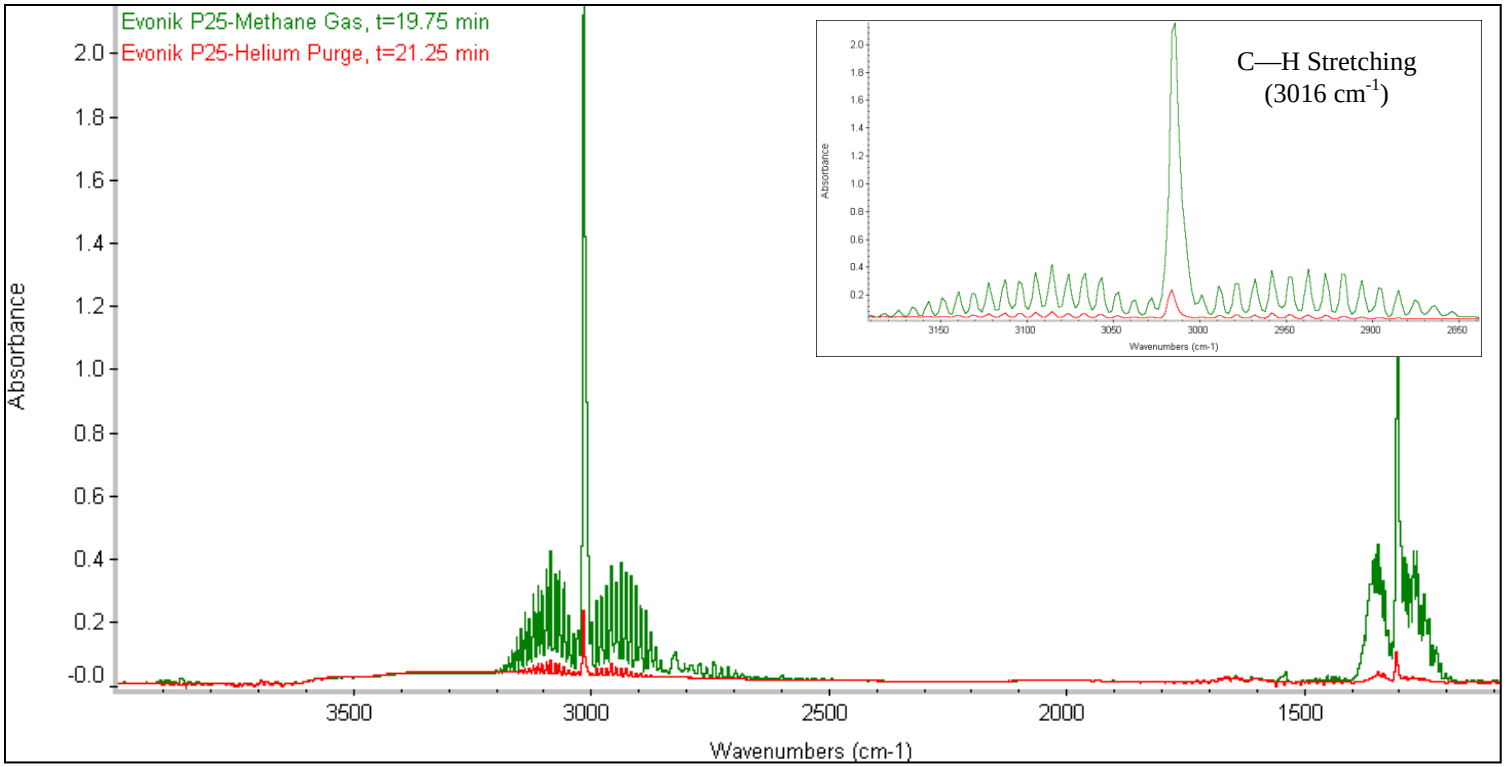

Figure 4.4-4 Experimental IR spectra of CH_4 adsorption-desorption on Evonik P25 TiO_2 with respect to time. (Characteristic feature of asymmetric C-H stretching is shown in inset figure).

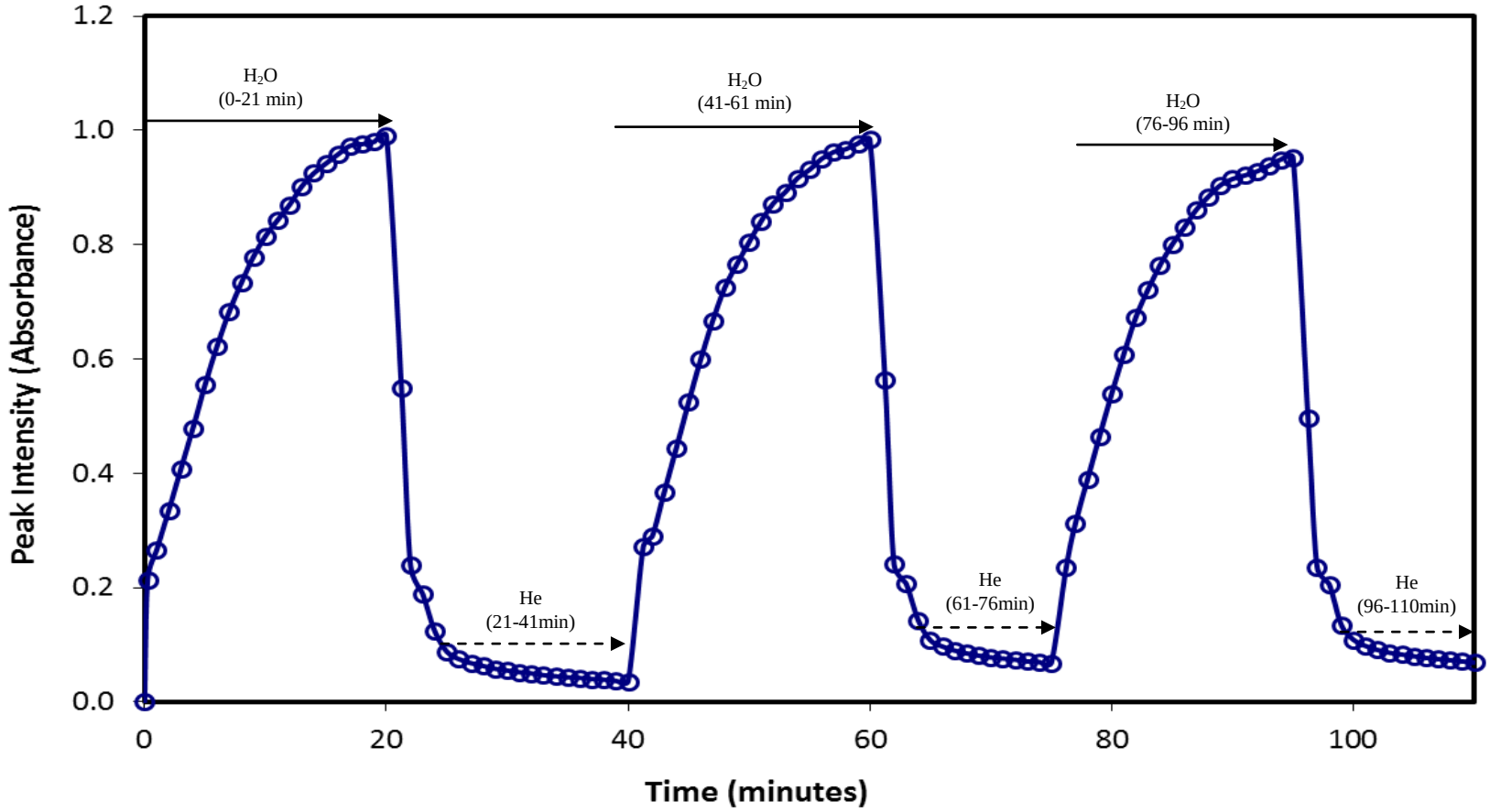

Figure 4.4-5 Adsorption-desorption plot of H_2O vapor on Evonik P25 TiO_2.

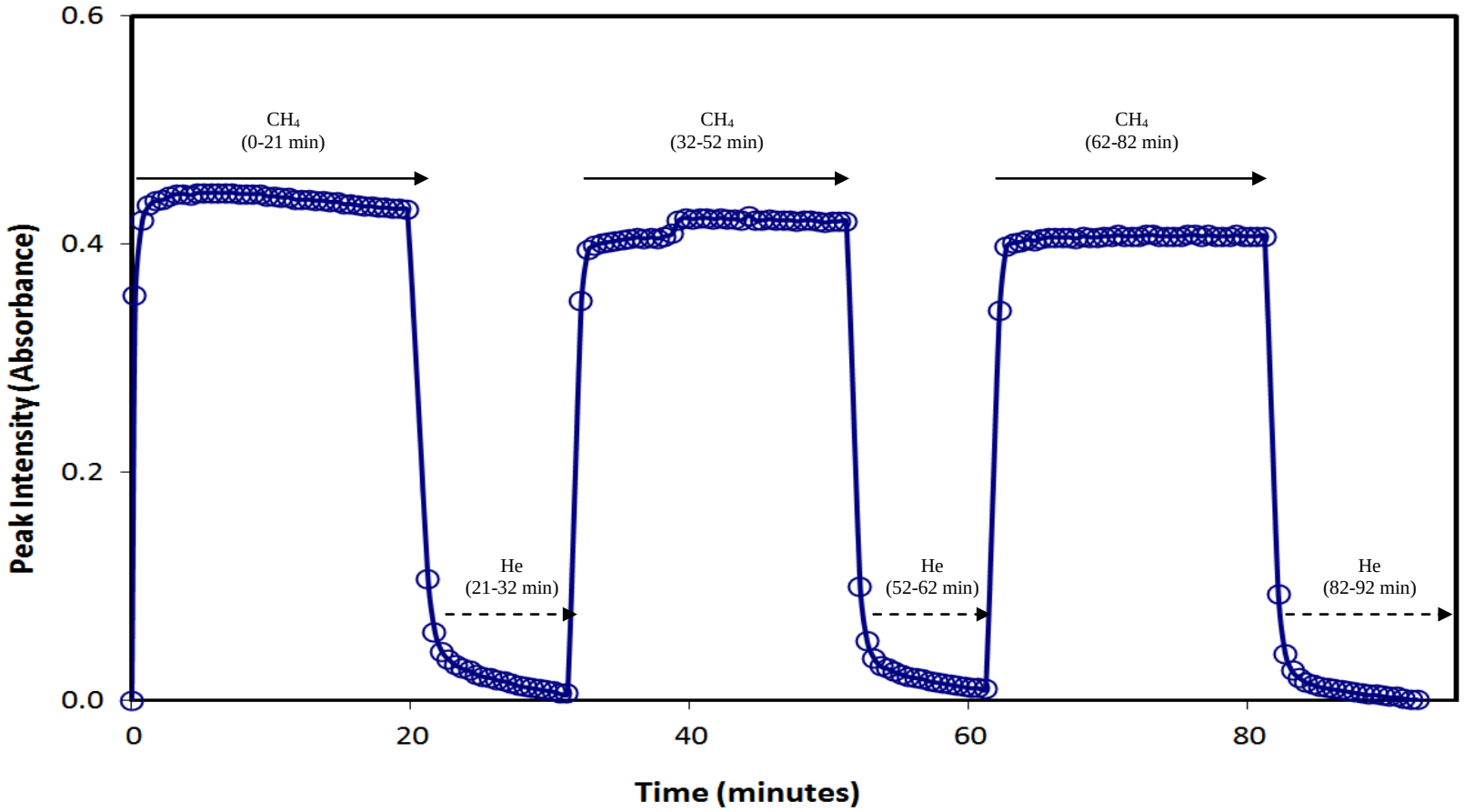

Figure 4.4-6 Adsorption-desorption plot of CH_4 gas on Evonik P25 TiO_2.

CHAPTER 5: DISCUSSION, CONCLUSIONS, AND FUTURE WORK

5.1 Discussion and Conclusions

Calculations derived from the computational study indicate all three molecules (CO, H_2O, and CH_4) adsorb more favorably onto the brookite TiO_2 (210) surface. As previously discussed in Section 2.4, the structural building of brookite (i.e. shorter interatomic distance, orthorhombic form) is believed to contribute to more favorable adsorption sites than the anatase polymorph. It is important to note that the prevalence of configurations on the brookite TiO_2 (210) surface is due to its asymmetrical layout. Computational results from this study indicate the brookite TiO_2 (210) surface exhibits additional binding configurations than for the anatase TiO_2 (101) surface. In all cases however, NBO charge analyses suggest insignificant charge transfer to the molecules occurs on neutral, negatively charged, positively charged, and V_o brookite TiO_2 (210) surfaces.

Four binding configurations (1A, 1B, 1C and 1D) were obtained for the CO molecule on neutral brookite TiO_2 (210). In the 1A and 1C configurations, the molecule is vertically oriented above the surface with the C atom directly above the Ti_{5c} site. The calculated BSSE corrected adsorption energies for both configurations ($\Delta E_{ads,A}$=-0.460eV, $\Delta E_{ads,C}$ = -0.600eV) suggest CO strongly adsorbs onto the surface. The configurations in which the CO molecule is vertically oriented above the surface with the O atom directly above the Ti_{5c} site (1B and 1D) demonstrate the adsorbate has less favorable adsorption energies. Results from the case in which CO interacts with a partially reduced (V_o) brookite

TiO_2 (210) surface (configurations 4A and 4B) show more favorable adsorption energies than those obtained from configurations on the neutral and negatively charged cluster.

Two binding configurations (1A and 1B) were obtained for the H_2O molecule on neutral brookite TiO_2 (210). In both configurations, the molecule is oriented above the surface with the O atom directly above the Ti_{5c} site. The calculated BSSE corrected adsorption energies for both configurations ($\Delta E_{ads,A}$ = -1.320eV, $\Delta E_{ads,B}$ = -1.763eV) suggest H_2O strongly adsorbs onto the surface. Results from the case in which H_2O interacts with a partially reduced (V_o) brookite TiO_2 (210) surface (configuration 4A) show more favorable adsorption energies than those obtained from on the neutral and negatively charged cluster. Provided that H_2O strongly binds to the brookite TiO_2 (210) surface, one can conclude that it plays a significant role in the surface reactions taking place on the surface. These results are in accordance with Anpo *et al*'s 1995 findings; wherein the addition of more H_2O in a CO_2 photoreduction reaction yields much higher concentrations of CH_4.

Two binding configurations (1A and 1B) were obtained for the CH_4 molecule on neutral brookite TiO_2 (210). In both configurations, the molecule is oriented above the surface with the C atom directly above the Ti_{5c} site. The calculated BSSE corrected adsorption energies for both configurations ($\Delta E_{ads,A}$ = -0.032eV, $\Delta E_{ads,B}$ = -0.108eV) suggest CH_4 weakly adsorbs onto the surface. Results from the case in which CH_4 interacts with a partially reduced (V_o) brookite TiO_2 (210) surface (configuration 4A) show slightly more favorable

adsorption energies than those obtained. Results from this study suggest that cases in which a brookite-containing material is not thermally treated (source of oxygen vacancies) a higher yield of CH_4 should occur. This is primarily due to weak interaction between CH_4 and the brookite TiO_2 (210) surface. Likewise, given that photocatalytic reactions are confined to the surface, the presence of oxygen vacancies in a brookite-containing material may lead to higher order (C_2) hydrocarbon formation.

The experimental results outlined in this thesis are well within agreement of the computational results. For instance, the theoretical vibrational frequencies for both H_2O and CH_4 on TiO_2 surfaces are in close agreement with to the experimental IR spectra generated from the adsorption-desorption studies. For example, O—H bending in the H_2O molecule was observed at 1652 cm^{-1} in the DRIFTS studies and at 1594 cm^{-1} and 1671 cm^{-1} for the computational studies. Asymmetrical stretching of the C—H bonds in the CH_4 molecule were observed at 3016 cm^{-1} experimentally and at 3012 cm^{-1} and 3019 cm^{-1} computationally.

As predicted computationally, the experimental work conducted in this study show that H_2O strongly binds onto TiO_2 surfaces. The constructed adsorption-desorption plot demonstrations that after one cycle (exposure to H_2O vapor then exposure to helium), approximately 13 percent of the Evonik P25 TiO_2 sample still contained H_2O on the surface. The adsorption-desorption plot of pure CH_4 gas on Evonik P25 TiO_2 is in strong agreement with the theoretical work; as both studies suggest CH_4 weakly binds onto TiO_2 surfaces. The absorbance intensity for CH_4 on Evonik P25 TiO_2 was found to be approximately half than

that of H_2O on Evonik P25 TiO_2 (0.4 vs. 1.0). After each cycle (exposure to CH_4 then exposure to helium), no traces of CH_4 gas were observed on the Evonik P25 TiO_2 sample.

The work outlined in this thesis provides a first account (from a theoretical standpoint) of adsorption behavior of CH_4 and CO molecules on the brookite TiO_2 surface. This in turn provides a constructive platform leading to a better understanding of the fundamental photocatalytic mechanisms taking place on a brookite-containing photocatalyst.

5.2 Implications for Future Work

The potential CO_2 conversion to fuels offers for meeting mounting energy demands with minimal environmental impact is great. Photocatalysis over Ti-based materials is a well-demonstrated and highly advantageous method utilized for CO_2 conversion to higher value products. While significant research and development has and continues to take place in the area of photocatalytic reduction of CO_2 and H_2O vapor to useful products (such as C_1-C_2 hydrocarbons) the application of this technology is limited due to various impediments. For example, enhancing the efficiency of the CO_2 photoreduction process on TiO_2 remains is a significant challenge. According to various sources from the literature, the efficiency of CO_2 photoreduction over Ti-based catalysts ranges from 0.00013 percent to 0.28 percent.[74,75] Designing more efficient Ti-based photocatalysts is one of the key approaches to enhancing the efficiency of CO_2 photoreduction in the presence of H_2O vapor. Moreover, an understanding of the

initial photoreduction pathways sets the groundwork for driving the production of desired products.

In light of the key points that were previously mentioned, future research should comprise of expanding computational and experimental studies. Implementing periodic DFT calculations of CO, H_2O, and CH_4 molecules on stoichiometric and defective (V_o) brookite TiO_2 (210) surfaces would serve as a means for obtaining a more thorough account of adsorption behaviors and interactions. Aside from the adsorption behavior of individual molecules on the periodic slab models, competitive adsorption of CO_2, CO, H_2O, and CH_4 molecules on the brookite TiO_2 (210) surface can also be investigated. Conducting a study as such would provide greater insight in developing reaction pathways associated with more practical conditions.

An experimental study conducted by Liu and collaborators substantiates CO_2^-, HCO_3^-, and HCOOH as key reaction intermediates for photoreduction of CO_2 with H_2O vapor on brookite surfaces.[65] Therefore, a theoretical investigation of the reaction intermediate, HCOOH, on the brookite TiO_2 (210) surface would help to further validate proposed reaction pathways in this work as well as in the literature. Periodic DFT work conducted by Li *et al*. is the first theoretical study of its kind to investigate HCOOH adsorption behavior on the brookite TiO_2 (210) surface.[46] The proposed future work could be executed in the same manner as Li *et al*. (e.g. periodic slab models) but with investigating the competitive adsorption behavior of HCOOH in the presence of other molecules.

Characterizing the adsorption and desorption behavior of reactants (CO_2, H_2O), and products (CO, CH_4) on untreated (stoichiometric) and treated (V_o) brookite-containing materials (pure and mixed-phase) is another feasible approach to future work. In essence, an experimental study utilizing DRIFTS would serve as a perfect means for executing this proposed work. Results from this type of study would provide a practical idea of how small molecules interact with brookite-containing materials. In summary, theoretical and experimental work outlining the competitive adsorption behavior of reactants, intermediates, and products on brookite TiO_2 materials serve as a significant basis for reaction prediction on these types of surfaces.

REFERENCES

1.U.S. Energy Information Administration *International Energy Outlook 2011*. 2011, *DOE/EIA-0484*.

2.Ekins, P., The secondary benefits of CO2 abatement: How much emission reduction do they justify? *Ecological Economics* 1996, 16, 13-24.

3.Fuhrer, J., Agroecosystern responses to combinations of elevated CO2, ozone, and global climate change. *Agriculture Ecosystems & Environment* 2003, 97, 1-20.

4.Jacobson, M. Z., Review of solutions to global warming, air pollution, and energy security. *Energy & Environmental Science* 2009, 2, 148-173.

5.Yang, H.; Xu, Z.; Fan, M.; Gupta, R.; Slimane, R. B.; Bland, A. E.; Wright, I., Progress in carbon dioxide separation and capture: A review. *Journal of Environmental Sciences-China* 2008, 20, 14-27.

6.Bentley, R. W., Global oil & gas depletion: an overview. *Energy Policy* 2002, 30, 189-205.

7.Managi, S.; Opaluch, J. J.; Jin, D.; Grigalunas, T. A., Technological change and depletion in offshore oil and gas. *Journal of Environmental Economics and Management* 2004, 47, 388-409.

8.Sorrell, S.; Speirs, J.; Bentley, R.; Brandt, A.; Miller, R., Global oil depletion: A review of the evidence. *Energy Policy* 2010, 38, 5290-5295.

9.White, C. M.; Smith, D. H.; Jones, K. L.; Goodman, A. L.; Jikich, S. A.; LaCount, R. B.; DuBose, S. B.; Ozdemir, E.; Morsi, B. I.; Schroeder, K. T., Sequestration of carbon dioxide in coal with enhanced coalbed methane recovery - A review. *Energy & Fuels* 2005, 19, 659-724.

10.Pires, J. C. M.; Martins, F. G.; Alvim-Ferraz, M. C. M.; Simoes, M., Recent developments on carbon capture and storage: An overview. *Chemical Engineering Research & Design* 2011, 89, 1446-1460.

11.Centi, G.; Perathoner, S., Opportunities and prospects in the chemical recycling of carbon dioxide to fuels. *Catalysis Today* 2009, 148, 191-205.

12.Wang, S. B.; Lu, G. Q. M.; Millar, G. J., Carbon dioxide reforming of methane to produce synthesis gas over metal-supported catalysts: State of the art. *Energy & Fuels* 1996, 10, 896-904.

13.Song, C. S., Global challenges and strategies for control, conversion and utilization of CO2 for sustainable development involving energy, catalysis, adsorption and chemical processing. *Catalysis Today* 2006, 115, 2-32.

14.Budzianowski, W. M., Value-added carbon management technologies for low CO2 intensive carbon-based energy vectors. *Energy* 2012, 41, 280-297.

15.de Richter, R.; Caillol, S., Fighting global warming: The potential of photocatalysis against CO2, CH4, N2O, CFCs, tropospheric O-3, BC and other major contributors to climate change. *Journal of Photochemistry and Photobiology C-Photochemistry Reviews* 2011, 12, 1-19.

16.Benson, E. E.; Kubiak, C. P.; Sathrum, A. J.; Smieja, J. M., Electrocatalytic and homogeneous approaches to conversion of CO2 to liquid fuels. *Chemical Society Reviews* 2009, 38, 89-99.

17.Fox, M. A.; Dulay, M. T., Heterogeneous Photocatalysis. *Chemical reviews* 1993, 93, 341-357.

18.Centi, G.; Perathoner, S., Catalysis: Role and Challenges for a Sustainable Energy. *Topics in Catalysis* 2009, 52, 948-961.

19.Centi, G.; Perathoner, S.; Rak, Z. S., Reduction of greenhouse gas emissions by catalytic processes. *Applied Catalysis B-Environmental* 2003, 41, 143-155.

20.Hagfeldt, A.; Gratzel, M., Light-Induced Redox Reactions in Nanocrystalline Systems. *Chemical reviews* 1995, 95, 49-68.

21.Mikkelsen, M.; Jorgensen, M.; Krebs, F. C., The teraton challenge. A review of fixation and transformation of carbon dioxide. *Energy & Environmental Science* 2010, 3, 43-81.

22.Hoffmann, M. R.; Martin, S. T.; Choi, W. Y.; Bahnemann, D. W., Environmental Applications of Semiconductor Photocatalysis. *Chemical reviews* 1995, 95, 69-96.

23.Shimizu, Y.; Egashira, M., Basic aspects and challenges of semiconductor gas sensors. *MRS Bulletin* 1999, 24, 18-24.

24.Fujishima, A.; Honda, K., Electrochemical Photolysis of Water at a Semiconductor Electrode. *Nature* 1972, 238, 37-+.

25.Centi, G.; Perathoner, S.; Wine, G.; Gangeri, M., Electrocatalytic conversion of CO2 to long carbon-chain hydrocarbons. *Green Chemistry* 2007, 9, 671-678.

26.Inoue, T.; Fujishima, A.; Konishi, S.; Honda, K., Photoelectrocatalytic Reduction of Carbon-Dioxide in Aqueous Suspensions of Semiconductor Powders. *Nature* 1979, 277, 637-638.

27.Anpo, M.; Yamashita, H.; Ichihashi, Y.; Fujii, Y.; Honda, M., Photocatalytic reduction of CO2 with H2O on titanium oxides anchored within micropores of zeolites: Effects of the structure of the active sites and the addition of Pt. *Journal of Physical Chemistry B* 1997, 101, 2632-2636.

28.Ikeue, K.; Nozaki, S.; Ogawa, M.; Anpo, M., Photocatalytic reduction of CO2 with H2O on Ti-containing porous silica thin film photocatalysts. *Catalysis Letters* 2002, 80, 111-114.

29.Ulagappan, N.; Frei, H., Mechanistic study of CO2 photoreduction in Ti silicalite molecular sieve by FT-IR spectroscopy. *Journal of Physical Chemistry a* 2000, 104, 7834-7839.

30.Tan, S. S.; Zou, L.; Hu, E., Photocatalytic reduction of carbon dioxide into gaseous hydrocarbon using TiO2 pellets. *Catalysis Today* 2006, 115, 269-273.

31.Lo, C.-C.; Hung, C.-H.; Yuan, C.-S.; Wu, J.-F., Photoreduction of carbon dioxide with H-2 and H2O over TiO2 and ZrO2 in a circulated photocatalytic reactor. *Solar Energy Materials and Solar Cells* 2007, 91, 1765-1774.

32.Xia, X.-H.; Jia, Z.-H.; Yu, Y.; Liang, Y.; Wang, Z.; Ma, L.-L., Preparation of multi-walled carbon nanotube supported TiO2 and its photocatalytic activity in the reduction of CO2 with H2O. *Carbon* 2007, 45, 717-721.

33.Wu, J. C. S.; Wu, T.-H.; Chu, T.; Huang, H.; Tsai, D., Application of optical-fiber photoreactor for CO(2) photocatalytic reduction. *Topics in Catalysis* 2008, 47, 131-136.

34.Varghese, O. K.; Paulose, M.; LaTempa, T. J.; Grimes, C. A., High-Rate Solar Photocatalytic Conversion of CO2 and Water Vapor to Hydrocarbon Fuels. *Nano Letters* 2009, 9, 731-737.

35.Wang, C.; Thompson, R. L.; Baltrus, J.; Matranga, C., Visible Light Photoreduction of CO2 Using CdSe/Pt/TiO2 Heterostructured Catalysts. *Journal of Physical Chemistry Letters* 2010, 1, 48-53.

36.Diebold, U., The surface science of titanium dioxide. *Surface Science Reports* 2003, 48, 53-229.

37.Landmann, M.; Rauls, E.; Schmidt, W. G., The electronic structure and optical response of rutile, anatase and brookite TiO2. *Journal of Physics-Condensed Matter* 2012, 24, 195503-195503.

38.Park, J.-Y.; Lee, C.; Jung, K.-W.; Jung, D., Structure Related Photocatalytic Properties of TiO2. *Bulletin of the Korean Chemical Society* 2009, 30, 402-404.

39.Mo, S. D.; Ching, W. Y., ELECTRONIC AND OPTICAL-PROPERTIES OF 3 PHASES OF TITANIUM-DIOXIDE - RUTILE, ANATASE, AND BROOKITE. *Physical Review B* 1995, 51, 13023-13032.

40.Mattsson, A.; Osterlund, L., Adsorption and Photoinduced Decomposition of Acetone and Acetic Acid on Anatase, Brookite, and Rutile TiO2 Nanoparticles. *Journal of Physical Chemistry C* 2010, 114, 14121-14132.

41.Asahi, R.; Taga, Y.; Mannstadt, W.; Freeman, A. J., Electronic and optical properties of anatase TiO2. *Physical Review B* 2000, 61, 7459-7465.

42.Bickley, R. I.; Gonzalezcarreno, T.; Lees, J. S.; Palmisano, L.; Tilley, R. J. D., A Structural Investigation of Titanium-Dioxide Photocatalysts. *Journal of Solid State Chemistry* 1991, 92, 178-190.

43.Acharya, D. P.; Camillone, N., III; Sutter, P., CO2 Adsorption, Diffusion, and Electron-Induced Chemistry on Rutile TiO2(110): A Low-Temperature Scanning Tunneling Microscopy Study. *Journal of Physical Chemistry C* 2011, 115, 12095-12105.

44.Gong, X.-Q.; Selloni, A., First-principles study of the structures and energetics of stoichiometric brookite TiO(2) surfaces. *Physical Review B* 2007, 76, 235307-235307.

45.Di Paola, A.; Addamo, M.; Bellardita, M.; Cazzanelli, E.; Palmisano, L., Preparation of photocatalytic brookite thin films. *Thin Solid Films* 2007, 515, 3527-3529.

46.Li, W.-K.; Gong, X.-Q.; Lu, G.; Selloni, A., Different reactivities of TiO2 polymorphs: Comparative DFT calculations of water and formic acid adsorption at anatase and brookite TiO2 surfaces. *Journal of Physical Chemistry C* 2008, 112, 6594-6596.

47.Indrakanti, V. P.; Kubicki, J. D.; Schobert, H. H., Photoinduced activation of CO2 on Ti-based heterogeneous catalysts: Current state, chemical physics-based insights and outlook. *Energy & Environmental Science* 2009, 2, 745-758.

48.Hurum, D. C.; Agrios, A. G.; Gray, K. A.; Rajh, T.; Thurnauer, M. C., Explaining the enhanced photocatalytic activity of Degussa P25 mixed-phase TiO2 using EPR. *Journal of Physical Chemistry B* 2003, 107, 4545-4549.

49.Li, G. H.; Ciston, S.; Saponjic, Z. V.; Chen, L.; Dimitrijevic, N. M.; Rajh, T.; Gray, K. A., Synthesizing mixed-phase TiO2 nanocomposites using a hydrothermal method for photo-oxidation and photoreduction applications. *Journal of Catalysis* 2008, 253, 105-110.

50.Hurum, D. C.; Gray, K. A.; Rajh, T.; Thurnauer, M. C., Recombination pathways in the Degussa P25 formulation of TiO2: Surface versus lattice mechanisms. *Journal of Physical Chemistry B* 2005, 109, 977-980.

51.Reddy, B. M.; Khan, A., Recent advances on TiO2-ZrO2 mixed oxides as catalysts and catalyst supports. *Catalysis Reviews-Science and Engineering* 2005, 47, 257-296.

52.Anpo, M.; Yamashita, H.; Ichihashi, Y.; Ehara, S., PHOTOCATALYTIC REDUCTION OF CO2 WITH H2O ON VARIOUS TITANIUM-OXIDE CATALYSTS. *Journal of Electroanalytical Chemistry* 1995, 396, 21-26.

53.Rasko, J., FTIR study of the photoinduced dissociation of CO2 on titania-supported noble metals. *Catalysis Letters* 1998, 56, 11-15.

54.Ramis, G.; Busca, G.; Lorenzelli, V., LOW-TEMPERATURE CO-2 ADSORPTION ON METAL-OXIDES - SPECTROSCOPIC CHARACTERIZATION OF SOME WEAKLY ADSORBED SPECIES. *Materials Chemistry and Physics* 1991, 29, 425-435.

55.Busca, G.; Lorenzelli, V., INFRARED SPECTROSCOPIC IDENTIFICATION OF SPECIES ARISING FROM REACTIVE ADSORPTION OF CARBON OXIDES ON METAL-OXIDE SURFACES. *Materials Chemistry* 1982, 7, 89-126.

56.He, H. Y.; Zapol, P.; Curtiss, L. A., A Theoretical Study of CO2 Anions on Anatase (101) Surface. *Journal of Physical Chemistry C* 2010, 114, 21474-21481.

57.Indrakanti, V. P.; Kubicki, J. D.; Schobert, H. H., Quantum chemical modeling of ground states of CO2 chemisorbed on anatase (001), (101), and (010) TiO2 surfaces. *Energy & Fuels* 2008, 22, 2611-2618.

58.Indrakanti, V. P.; Schobert, H. H.; Kubicki, J. D., Quantum Mechanical Modeling of CO2 Interactions with Irradiated Stoichiometric and Oxygen-Deficient Anatase TiO2 Surfaces: Implications for the Photocatalytic Reduction of CO2. *Energy & Fuels* 2009, 23, 5247-5256.

59.Indrakanti, V. P.; Kubicki, J. D.; Schobert, H. H., Photoinduced activation of CO2 on TiO2 surfaces: Quantum chemical modeling of CO2 adsorption on oxygen vacancies. *Fuel Processing Technology* 2011, 92, 805-811.

60.Shibata, T.; Irie, H.; Ohmori, M.; Nakajima, A.; Watanabe, T.; Hashimoto, K., Comparison of photochemical properties of brookite and anatase TiO2 films. *Physical Chemistry Chemical Physics* 2004, 6, 1359-1362.

61.Iskandar, F.; Nandiyanto, A. B. D.; Yun, K. M.; Hogan, C. J.; Okuyama, K.; Biswas, P., Enhanced photocatalytic performance of brookite TiO2 macroporous particles prepared by spray drying with colloidal templating. *Advanced Materials* 2007, 19, 1408-+.

62.Yan, W. F.; Chen, B.; Mahurin, S. M.; Dai, S.; Overbury, S. H., Brookite-supported highly stable gold catalytic system for CO oxidation. *Chemical Communications* 2004, 1918-1919.

63.Ardizzone, S.; Bianchi, C. L.; Cappelletti, G.; Gialanella, S.; Pirola, C.; Ragaini, V., Tailored anatase/brookite nanocrystalline TiO2. The optimal particle features for liquid- and gas-phase photocatalytic reactions. *Journal of Physical Chemistry C* 2007, 111, 13222-13231.

64.Li, W.-K.; Chu, L.-N.; Gong, X.-Q.; Lu, G., A comparative DFT study of adsorption and catalytic performance of Au nanoparticles at anatase and brookite TiO2 surfaces. *Surface Science* 2011, 605, 1369-1380.

65.Liu, L.; Zhao, H.; Andino, J.; Li, Y., Photocatalytic CO2 Reduction with H2O on TiO2 Nanocrystals: Comparison of Anatase, Rutile, and Brookite Polymorphs and Exploration of Surface Chemistry. *ACS Catalysis* 2012.

66.Wanbayor, R.; Ruangpornvisuti, V., Adsorption of di-, tri- and polyatomic gases on the anatase TiO2 (001) and (101) surfaces and their adsorption abilities. *Journal of Molecular Structure-Theochem* 2010, 952, 103-108.

67.Wanbayor, R.; Ruangpornvisuti, V., Adsorption of CO, H-2, N2O, NH3 and CH4 on the anatase TiO2 (001) and (101) surfaces and their competitive adsorption predicted by periodic DFT calculations. *Materials Chemistry and Physics* 2010, 124, 720-725.

68.Pipornpong, W.; Wanbayor, R.; Ruangpornvisuti, V., Adsorption CO2 on the perfect and oxygen vacancy defect surfaces of anatase TiO2 and its photocatalytic mechanism of conversion to CO. *Applied Surface Science* 2011, 257, 10322-10328.

69.Nik, E. B.; Sadighi-Bonabi, R., Theoretical study of CO adsorption on the illuminated TiO2 (001) surface. *Applied Surface Science* 2010, 256, 3795-3798.

70.Frisch, M. J.; Trucks, G. W.; Schlegel, H. B.; Scuseria, G. E.; Robb, M. A.; Cheeseman, J. R.; Montgomery, J., J. A.; Vreven, T.; Kudin, K. N.; Burant, J. C.; Millam, J. M.; Iyengar, S. S.; Tomasi, J.; Barone, V.; Mennucci, B.; Cossi, M.; Scalmani, G.; Rega, N.; Petersson, G. A.; Nakatsuji, H.; Hada, M.; Ehara, M.; Toyota, K.; Fukuda, R.; Hasegawa, J.; Ishida, M.; Nakajima, T.; Honda, Y.; Kitao, O.; Nakai, H.; Klene, M.; Li, X.; Knox, J. E.; Hratchian, H. P.; Cross, J. B.; Bakken, V.; Adamo, C.; Jaramillo, J.; Gomperts, R.; Stratmann, R. E.; Yazyev, O.; Austin, A. J.; Cammi, R.; Pomelli, C.; Ochterski, J. W.; Ayala, P. Y.; Morokuma, K.; Voth, G. A.; Salvador, P.; Dannenberg, J. J.; Zakrzewski, V. G.; Dapprich, S.; Daniels, A. D.; Strain, M. C.; Farkas, O.; Malick, D. K.; Rabuck, A. D.; Raghavachari, K.; Foresman, J. B.; Ortiz, J. V.; Cui, Q.; Baboul, A. G.; Clifford, S.; Cioslowski, J.; Stefanov, B. B.; Liu, G.; Liashenko, A.; Piskorz, P.; Komaromi, I.; Martin, R. L.; Fox, D. J.; Keith, T.; Al-Laham, M. A.; Peng, C. Y.; Nanayakkara, A.; Challacombe, M.; Gill, P. M. W.; Johnson, B.; Chen, W.; Wong, M. W.; Gonzalez, C.; and Pople, J. A. Gaussian, Inc., Wallingford CT, 2004.

71.Boys, S. F.; Bernardi, F., The calculation of small molecular interactions by the differences of separate total energies. Some procedures with reduced errors (Reprinted from Molecular Physics, vol 19, pg 553-566, 1970). *Molecular Physics* 2002, 100, 65-73.

72.Lindan, P. J. D.; Harrison, N. M.; Holender, J. M.; Gillan, M. J., First-principles molecular dynamics simulation of water dissociation on TiO2(110). *Chemical Physics Letters* 1996, 261, 246-252.

73.Verhoef, R. W.; Kelly, D.; Mullins, C. B.; Weinberg, W. H., DIRECT DISSOCIATIVE CHEMISORPTION OF METHANE AND ETHANE ON IR(110) - ISOTOPE EFFECTS AND VIBRATIONALLY ASSISTED CHEMISORPTION. *Surface Science* 1994, 311, 196-213.

74.Indrakanti, V. P. Photoinduced activation of CO2 on TiO2 surfaces: Quantum chemical modeling of ground and excited states, and in situ EPR studies. Pennsylvania State University, 2009.

75.Roy, S. C.; Varghese, O. K.; Paulose, M.; Grimes, C. A., Toward Solar Fuels: Photocatalytic Conversion of Carbon Dioxide to Hydrocarbons. *Acs Nano* 2010, 4, 1259-1278.